Title
A Computational Fluid Dynamic Investigation of Hydrodynamic Interactions between Respiratory Flows and Circum-Pectoral Fin Flows in Labriform-Swimming Fishes

Author
Leung, David

Publication Date
2018

UNIVERSITY OF CALIFORNIA
Los Angeles

A Computational Fluid Dynamic Investigation of Hydrodynamic Interactions between Respiratory Flows and Circum-Pectoral Fin Flows in Labriform-Swimming Fishes

A thesis submitted in partial satisfaction
of the requirements for the degree
Master of Science in Mechanical Engineering

by

David Leung

2018

ABSTRACT OF THE THESIS

A Computational Fluid Dynamic Investigation of Hydrodynamic Interactions between Respiratory Flows and Circum-Pectoral Fin Flows in Labriform-Swimming Fishes

by

David Leung
Master of Science in Mechanical Engineering
University of California, Los Angeles, 2018
Professor Jeffery D. Eldredge, Chair

Hydrodynamic interactions between respiratory fluid flows leaving the opercular openings and flows around the closely downstream pectoral fins of fishes are poorly understood. Labriform-swimming fishes that swim primarily by moving only their pectoral fins are good subjects for such studies. We did a high-fidelity two-dimensional computational investigation of these interactions using normal respiratory movements in both resting and slow steady swimming conditions based on representative values for parameters taken from experimental and computational work on the bluegill sunfish (*Lepomis macrochirus*) and largemouth bass (*Micropterus salmoides*). We did a parametric study investigating the effects varying swimming speeds, strengths of opercular flows, and phase differences between pectoral fin and opercular opening and closing movements have on the thrust and side slip forces generated by the pectoral fins during both abduction and adduction portions of movement cycles. We analyzed pressure distributions on fin surfaces to determine physical differences in flows with and without opercular openings. Complex flow structures emerged from the coupling between opercular jets and vortex shedding from pectoral fins. The jets from the opercular opening appear to exert significant influence on the forces generated by the fins. These simulations and corresponding analysis establish a framework for study of these interactions in various labriform swimmers in a variety of flow regimes. These processes are likely significant in the maneuverability of these fishes.

The thesis of David Leung is approved.

Hossein Pirouz Kavehpour

Malcolm S. Gordon

Jeffery D. Eldredge, Committee Chair

University of California, Los Angeles

2018

TABLE OF CONTENTS

LIST OF FIGURES

LIST OF TABLES

ACKNOWLEDGMENTS

First and foremost, I would like to thank my advisor and committee chair, Professor Jeff Eldredge, for his mentorship and guidance. This thesis would not have been possible without his constant encouragement and support. I am also especially grateful for the help and support of Professor Malcolm Gordon, whose invaluable knowledge in fish biology was helpful throughout my research. Moreover, I would like to thank Professor Pirouz Kavehpour for taking the time in his schedule to serve on my committee.

In addition, I am also sincerely grateful for my friends, family, and girlfriend. I would especially like to thank my mom, dad, and sister for their unconditional love and continued encouragement throughout my studies and life. Last but not least, I want to thank my girlfriend, Melody, for her unwavering support and understanding throughout this process. Thank you all.

CHAPTER 1

Introduction

Many underwater robotic vehicles mimic fish locomotion since fish swim very efficiently. Thus, it is important to understand fish locomotion to effectively design bioinspired robotics. Although fish swim in a variety of different ways, around 90% of fish have pectoral fins and breathe by passing water through their gills. Anatomically, these gills are just forward of the pectoral fins and water leaving the gills through the opercular opening will interact with the pectoral fins, as seen in Figure 1.1. This interaction can potentially affect the forces pectoral fins generate. These forces are typically important for stability and maneuverability, though they can also be important for propulsion.

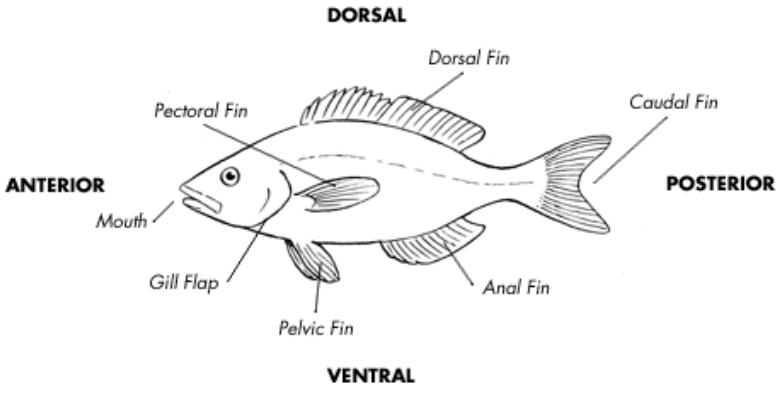

Figure 1.1: Fins of a Fish[1]

There has been extensive research done on both fish respiration and labriform swimming, where fish swim primarily using only their pectoral fins. For example, Evans et al. investigated the anatomy of fish gills and their function in gas exchange during respiration (Evans

[1]From `http://www.pbs.org/wgbh/nova/education/activities/3003_fish_01.html`

et al., 2005). Before this, Hughes modeled the respiratory process as a periodic dual pump system, where water leaves the opercular opening due to a pressure difference in the buccal cavity and the opercular cavity (Hughes, 1968).

In addition, Mittal et al. used computational fluid dynamics to analyze the forces generated by a flexible three-dimensional bluegill sunfish (*Lepomis macrochirus*), a common labriform-swimming fish. Moreover, Lauder et al. used particle image velocimetry (PIV) to experimentally visualize and analyze actual bluegill sunfish.

However, no one to date has combined these topics and studied the interaction between respiratory flows leaving the opercular opening and flows created by pectoral fins. In the present study, we investigate this interaction to see how it affects the thrust and side slip forces generated by pectoral fins during slow respiratory swimming. We simulated and analyzed a simplified model of a labriform-swimming fish since labriform swimmers are naturally most affected by this interaction. Since fish can swim using a variety of different flow patterns and regimes, we did a parametric study with this simplified model varying important dimensionless parameters to encompass the variability in fish. Although this simplified model doesn't exactly replicate the kinematics of a labriform-swimming fish, analyzing a simplified model gives us initial insight as to whether or not this interaction significantly affects the forces generated by pectoral fins and is worth further investigation.

This thesis is organized as follows: Chapter 2 goes through the assumptions and methodology for both the initial simulation and parametric study to model this interaction. Chapter 3 presents the results of the study and talks about what they mean. Finally, Chapter 4 summarizes the main findings from the thesis and discusses future steps to extend this work.

CHAPTER 2

Methodology

2.1 Overview and Assumptions

The pectoral fins of a generic labriform-swimming fish were modeled as rigid and two-dimensional axisymmetric to lower computational cost and simplify analysis while keeping the main characteristics of labriform swimming. While pectoral fins are flexible and three-dimensional in nature, this simplified model sets up a framework to analyze trends in varying key parameters of fish rather than attempts to model the exact behavior and motion of labriform-swimming fish. The two-dimensional axisymmetric assumption was used since fish often perform symmetrical movements on both their left and right sides. In addition, the rigidity assumption was used since the pectoral fin and respiratory flow interaction occurs mainly at the base of the pectoral fin, which is fairly rigid in nature. This assumption, however, incorrectly predicts the forces generated by the pectoral fin. This is especially true during the upstroke (abduction) portion of the pectoral fin movement cycle since a rigid fin eventually produces drag during this phase while an actual labriform swimmer produces thrust throughout the entire abduction and adduction movement cycle (Mittal et al., 2006).

Given these assumptions, we used this model to run an initial computational fluid dynamic simulation in COMSOL Multiphysics® using geometric and flow parameters based on previous research on bluegill sunfish and largemouth bass (*Micropterus salmoides*). We then varied dimensionless flow parameters from this initial case and investigated trends in the thrust and side slip forces generated by the model fish. This analysis gives a first look into this phenomena to see if it is important and should be further investigated. Future studies can improve on this work by extending the model to a flexible 3D pectoral fin.

2.2 Geometry and Mesh

Figure 2.1 shows the resulting geometry under these assumptions. This geometry is 2D-axisymmetric from a top-down view, modeling only the left hand side of the fish. The fish swims in the negative x direction as its pectoral fin oscillates back and forth. The opercular opening was modeled as a long channel where the end opens and closes in an oscillatory motion. The length of this channel was chosen so that the flow from the opercular opening is fully developed while the width of the channel was chosen to approximately match a fully opened gill cover. The approximate dimensions of the pectoral fin as well as the location of the opercular opening and other important parameters were chosen to roughly match that of a bluegill sunfish. These dimensions are shown in Table 2.1.

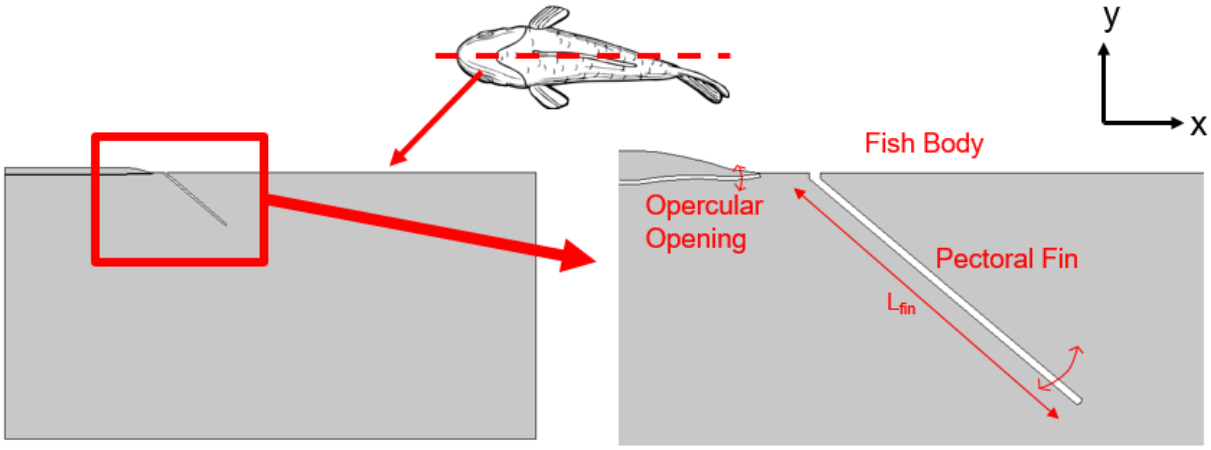

Figure 2.1: Simulation Geometry

The resulting geometry was meshed with triangular elements for ease of use and computational speed. The mesh was further refined near the pectoral fin tip and opercular opening since these locations have complicated flow physics that needs to be resolved. This mesh is shown in Figure 2.2. A mesh refinement test was done by using the same generic mesh setup (i.e. more refined in certain regions), but increasing the overall number of elements in the mesh and re-computing the solution. This was done until the pressure distribution along the pectoral fin at each instant was roughly the same by visual inspection even if the number of elements was increased, as seen in Figure 2.3. Only the pressure on the outer portion for

Table 2.1: Parameters of Fish. N/A Means Data Was Not Found in the Papers

Parameter	Bluegill Sunfish (Lauder et al., 2006)	Largemouth Bass (Lauder et al., 1984)	Initial Simulation
ρ	1000 kg/m^3	1000 kg/m^3	1000 kg/m^3
μ	1e-3 $kg/m/s$	1e-3 $kg/m/s$	1e-3 $kg/m/s$
ΔP	N/A	50 Pa	2 Pa
f_{fin}	2.17 $1/s$	1 $1/s$	0.1 $1/s$
f_{op}	N/A	N/A	0.1 $1/s$
L_{fin}	0.04 m	0.04 m	0.045 m
U_{swim}	0.16 m/s	N/A	0.01125 m/s
$\theta_{o,fin}$	N/A	N/A	-40°
$\theta_{r,fin}$	N/A	N/A	35°
$\theta_{o,op}$	N/A	N/A	0°
$\theta_{r,op}$	N/A	N/A	-35°
$Re_{fintip} = \frac{\rho f_{fin} L_{fin}^2}{\mu}$	3472	1600	202.5
$Re = \frac{\rho U_{swim} L_{fin}}{\mu}$	6400	N/A	506.25
$Dim.\, Pressure = \frac{\Delta P}{\rho f_{fin}^2 L_{fin}^2}$	N/A	31.25	98.7654
$St = \frac{f_{fin} L_{fin}}{U_{swim}}$	0.543	N/A	0.4

the pectoral fin (0 m at base, 0.045 m at tip) was plotted since this is the side where the pectoral fin interacts with the respiratory flow.

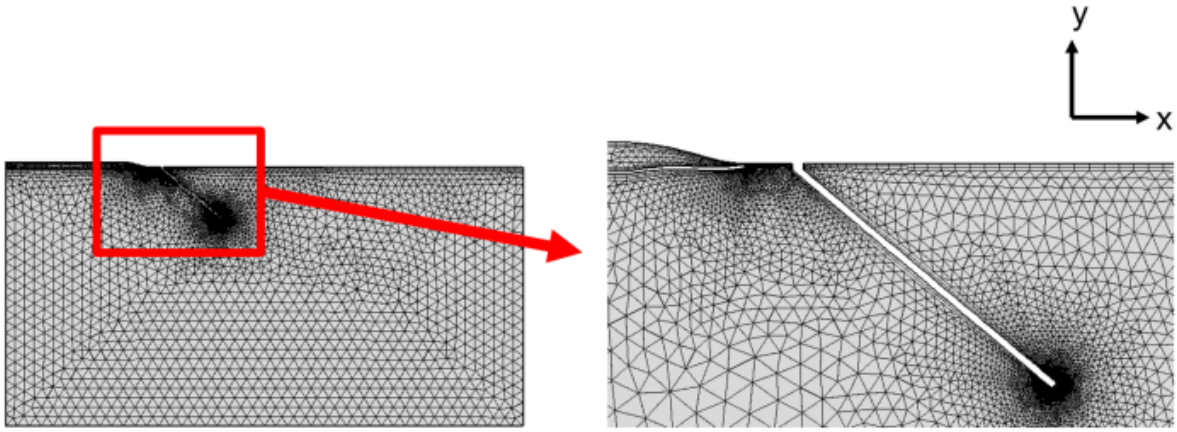

Figure 2.2: Simulation Mesh

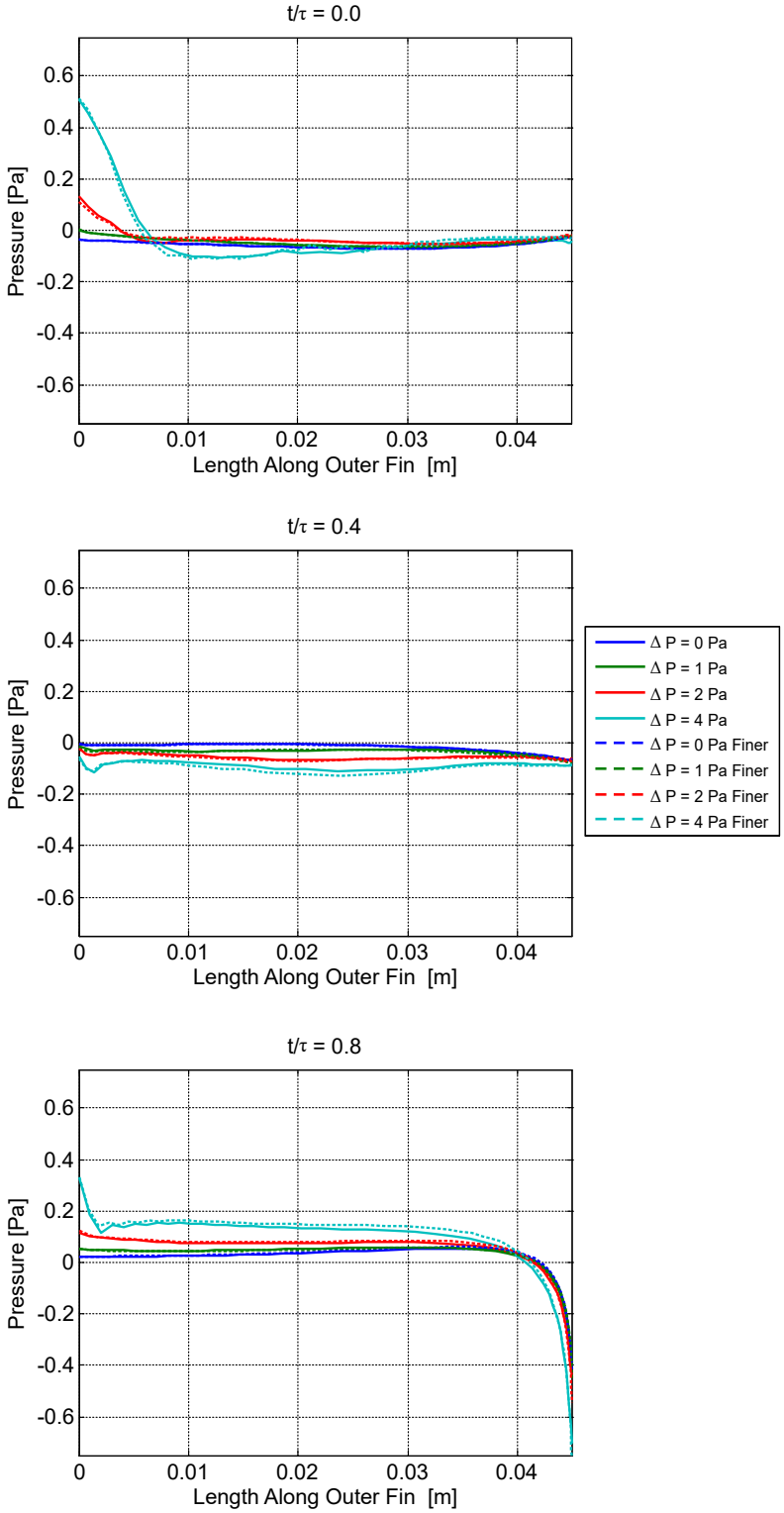

Figure 2.3: Mesh Independence Test for Various Times Throughout the Pectoral Fin Movement Cycle

2.3 Boundary and Initial Conditions

Five main boundary conditions were used for this simulation, as seen in Figure 2.4. First, the fish body was modeled as a wall, which enforces the no slip and no flow through conditions. The pectoral fin and opercular opening were modeled as moving walls, which oscillate in a back and forth motion while continuously enforcing the no slip and no flow through conditions. The rigid body oscillation was determined in COMSOL Multiphysics® by specifying the velocity at each point of the discretized pectoral fin and opercular opening, as seen in Equation 2.1. This was calculated by knowing the oscillatory movement (magnitude and phase) of the pectoral fin ($\theta_{z,fin}$) and opercular opening ($\theta_{z,op}$), as seen in Equation 2.2, as well as by knowing the x and y locations of the pivot point (x_p, y_p) for each of these movements. For example, if we know that the rigid pectoral fin oscillates 35 degrees back and forth about its base at a frequency of 0.1 Hz, we can use Equation 2.1 to specify velocity in COMSOL Multiphysics®. Since this boundary moves, the built in Arbitrary Lagrangian-Eulerian re-meshing scheme in COMSOL Multiphysics® was implemented to re-mesh the geometry after a specified distortion of the mesh.

$$\begin{bmatrix} u_j \\ v_j \end{bmatrix} = \dot{\theta} z \begin{bmatrix} -(y_j - y_p) \\ (x_j - x_p) \end{bmatrix} \tag{2.1}$$

Where x_j and y_j are the x and y coordinates of the discretized oscillating geometry, u_j and v_j are the corresponding x and y component of velocity at (x_j,y_j), and x_p and y_p are the x and y coordinates of the pivot point about which the geometry rotates.

$$\theta_z(t) = \theta_r \sin(2\pi f t + \phi) \tag{2.2}$$

Where θ_r is how much the rigid body will rotate, f is the frequency at which it rotates [Hz], and ϕ is any phase offset for the rigid body rotation. For these simulations, a positive phase difference denotes the pectoral fin oscillation leading the opercular opening oscillation, as seen in Figure 2.5.

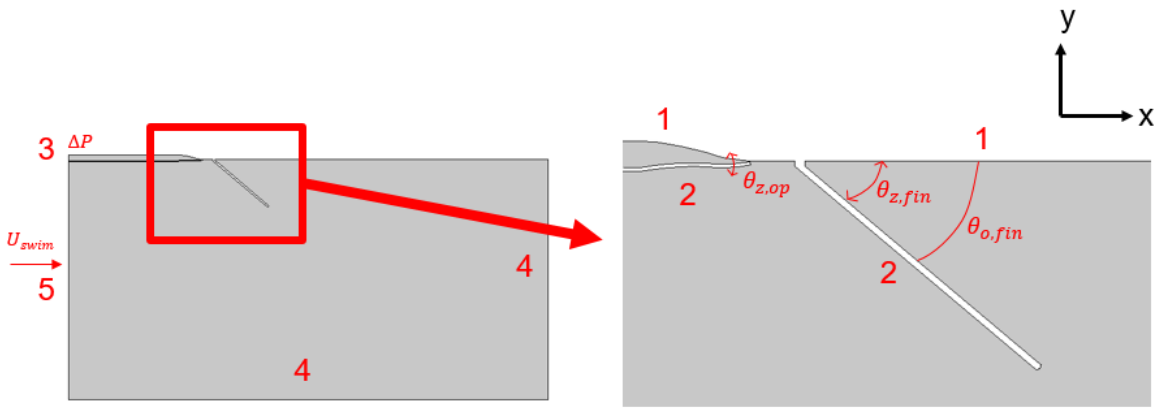

Figure 2.4: Boundary Conditions for Simulation. 1: Wall, 2: Moving Wall (Oscillatory), 3: Pressure Inlet, 4: Pressure Outlet, 5: Velocity Inlet

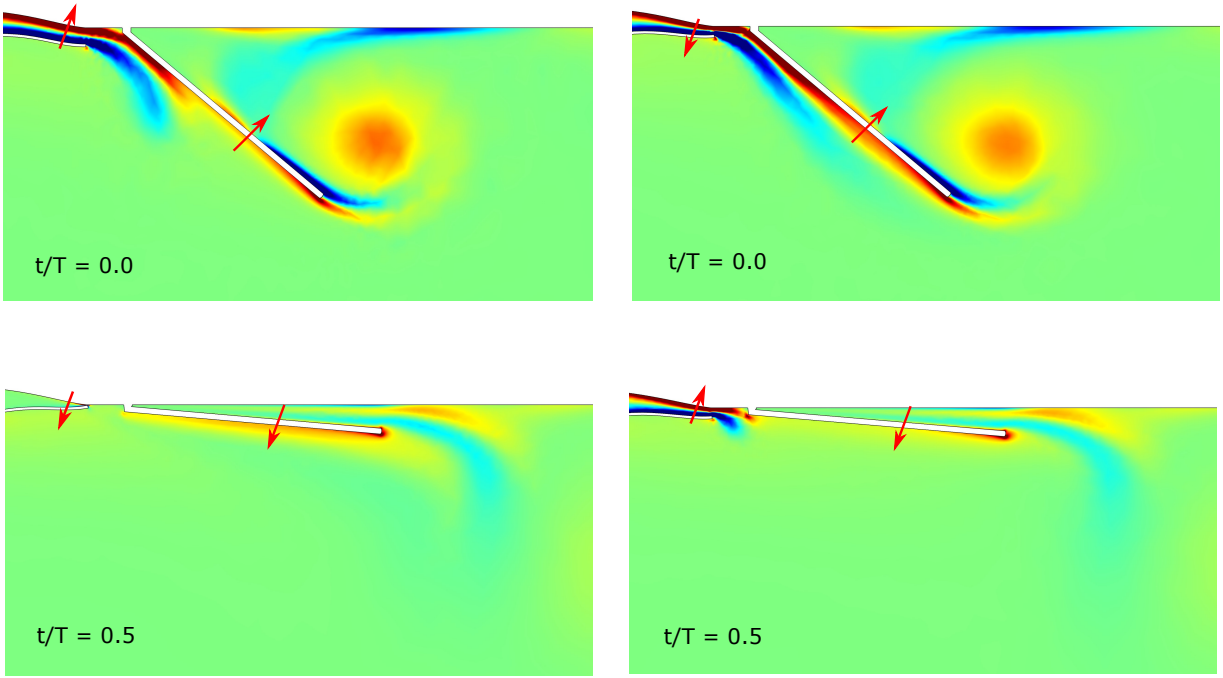

Figure 2.5: Vorticity Surface Plots at the Beginning and Middle of the Pectoral Fin Movement Cycle for 0° Offset (Left) and 90° Offset (Right). Arrows Denote Direction of Movement as t/τ Increases

The rightmost and bottommost boundaries far away from fish body were treated as pressure outlets, so that the boundaries would not interfere with the physics involved near the fish. The flow from the opercular opening was modeled as a channel with a specified inlet pressure. This inlet pressure specifies how fast water leaves the gills since the pressure difference (ΔP) in the channel drives the flow. Opening and closing the opercular opening with a fixed pressure difference mimics the oscilating pressure profile seen in fish since the velocity leaving the opening is only a function of the pressure and area via Bernoulli's equation. Thus, both an oscillatory pressure or opening area profile will produce an oscillatory velocity profile leaving the gills. Finally, the leftmost wall was treated as a velocity inlet flowing normal to the boundary to specify a specific swimming speed (U_{swim}) for the fish.

The initial condition was chosen as having zero velocity in each direction at each spatial point since the flow was not known beforehand. The simulation was run until there were no changes in the pressure distribution along the fin at each instant from one pectoral fin movement cycle to the next. This ensured that the flow reached steady state and did not depend on the initial conditions.

2.4 Flow Parameters

We also modeled the main flow characteristics of a fish based on typical values for a bluegill sunfish and largemouth bass, as seen in Table 2.1. We were interested in directly comparing Reynolds Number (Re), Strouhal Number (St), and a dimensionless pressure for a typical labriform-swimming fish to the equivalent dimensionless parameters for our initial simulation. These are defined as follows:

$$Re = \frac{\rho U_{swim} L_{fin}}{\mu} \tag{2.3}$$

$$Re_{fin\,tip} = \frac{\rho f_{fin} L_{fin}^2}{\mu} \tag{2.4}$$

$$Dimensionless\ Pressure = \frac{\Delta P}{\rho f_{fin}^2 L_{fin}^2} \tag{2.5}$$

$$St = \frac{f_{fin} L_{fin}}{U_{swim}} \tag{2.6}$$

Where ρ is the density of water, U_{swim} is the fish swimming speed, L_{fin} is the length of the pectoral fin, μ is the viscosity of water, f_{fin} is the pectoral fin beat frequency, and ΔP is the specified pressure difference to drive the opercular jet flow.

Re is defined as the ratio between the inertial forces and viscous forces using the freestream swimming velocity U_{swim}, $Re_{fin\,tip}$ is the ratio between the inertial forces and viscous forces using the pectoral fin tip velocity, dimensionless pressure is the ratio between the prescribed pressure difference in the opercular cavity and the dynamic pressure from the pectoral fin tip velocity, and St is the ratio between the pectoral fin tip velocity and freestream swimming velocity.

2.5 COMSOL Multiphysics® Solver

In COMSOL Multiphysics®, we set up a time dependent, incompressible, laminar, single phase flow solver, which uses BDF second order time stepping in finite element formulation using the parameters outlined above. COMSOL Multiphysics® ultimately solves the coupled Navier-Stokes and continuity equations, shown in Equations 2.7 and 2.8, under the conditions outlined before.

$$\rho \frac{D\vec{u}}{Dt} = -\nabla P + \rho \vec{g} + \mu \nabla^2 \vec{u} \tag{2.7}$$

$$\nabla \cdot \vec{u} = 0 \tag{2.8}$$

Where $\vec{u}$ is the velocity vector, ∇P is the pressure gradient, $\vec{g}$ is the gravity vector, and ρ and μ are the density and viscosity of the fluid.

2.6 Initial Simulation

In the initial simulation, we chose flow parameters to approximately match a slow moving labriform swimmer during respiration. This resulted in the model fish pectoral fin oscillating at a frequency of 0.1 Hz with a swimming speed of 0.01125 m/s, as seen in Table 2.1. We modeled the pectoral fin to start open with $\theta_{o,fin}$ = -40° and rotate 35° toward the body and back, as seen in Figure 2.4.

We also modeled the opercular opening to oscillate in phase with the pectoral fin at 0.1 Hz. While the relationship between the motion of the opercular opening and pectoral fin is not known, the frequency of oscillation for the opercular opening should be on the same order of magnitude as the pectoral fin beat frequency. The opercular opening started closed with $\theta_{o,op} = 0°$ and rotated -35° away from the body and back. To get the pectoral fin and opercular opening motions in phase with each other, the motion of the opercular opening was delayed until it matched with the pectoral fin motion.

These flow parameters yield approximately $1/12^{\text{th}}$ of the Reynolds Number for a slow swimming bluegill sunfish, as seen in Table 2.1. This was done because it has been shown that the main flow characteristics for labriform swimming have a weak relationship with Re, and simulating a lower Re saves having to resolve smaller scales of the flow (Mittal et al., 2006). The simulated Strouhal Number, on the other hand, approximately matched that of a bluegill sunfish moving at 0.16 m/s (1.1 L/s), as seen in Table 2.1.

The pressure drop (ΔP) in the opercular channel was chosen as 2 Pa, resulting in a dimensionless pressure slightly higher (but on the same order of magnitude) as that of a largemouth bass, as seen in Table 2.1. The frequency used for this calculation was the frequency of the largemouth bass's opercular opening motion rather than its pectoral fin beat frequency since the frequency of the largemouth bass's pectoral fin was not measured.

Videos of surface plots of vorticity for the initial simulation can be seen in supplemental material. A description of these videos can be found in the Appendix. For each case, density and viscosity were approximated as that of water.

2.7 Parametric Study

The parameters used in the initial simulation are approximate for a slow moving fish during respiration. Since different fish can move at various flow regimes and in general have different movement patterns than a bluegill sunfish, we performed a parametric study varying several key parameters of the flow to encompass a wide variety of fish species and flow regimes. The varying parameters are given in Table 2.2, while the enforced swimming speeds corresponding to the varying St are given in Table 2.3. This parametric study will show trends in varying key parameters of the fish and flow.

Table 2.2: Parametric Study Values

Parameter	Values
ΔP	0 Pa, 1 Pa, 2 Pa, 4 Pa, 6 Pa, 8 Pa
Phase Difference	-180°, -135°, -90°, -45°, 0°, 45°, 90°, 135°
St	0.1, 0.15, 0.175, 0.2, 0.25, 0.3, 0.4, 0.6

Table 2.3: Swimming Speed for Given St, for Fish Parameters Given in Table 2.1

St	U_{swim}
0.1	0.045 m/s
0.15	0.03 m/s
0.175	0.0257 m/s
0.2	0.0225 m/s
0.25	0.018 m/s
0.3	0.015 m/s
0.4	0.01125 m/s
0.6	0.0075 m/s

2.8 Post Processing

We were most interested in how the opercular jet flow affects both the thrust and side slip forces generated by the pectoral fin. To determine the thrust and side slip forces, we numerically integrated pressure along the fin using the trapezoidal rule and found each component of the force from Equation 2.9, assuming that only pressure contributes to the force. The force in the negative x direction was computed as thrust and the force in the y direction was computed as side slip. For the computation, the normal vector for the discretized i^{th} point was taken to be the normal vector corresponding to the vector created by the i-1 and i+1 points, as seen in Figure 2.6. The force data was then filtered using a five point time average of the data.

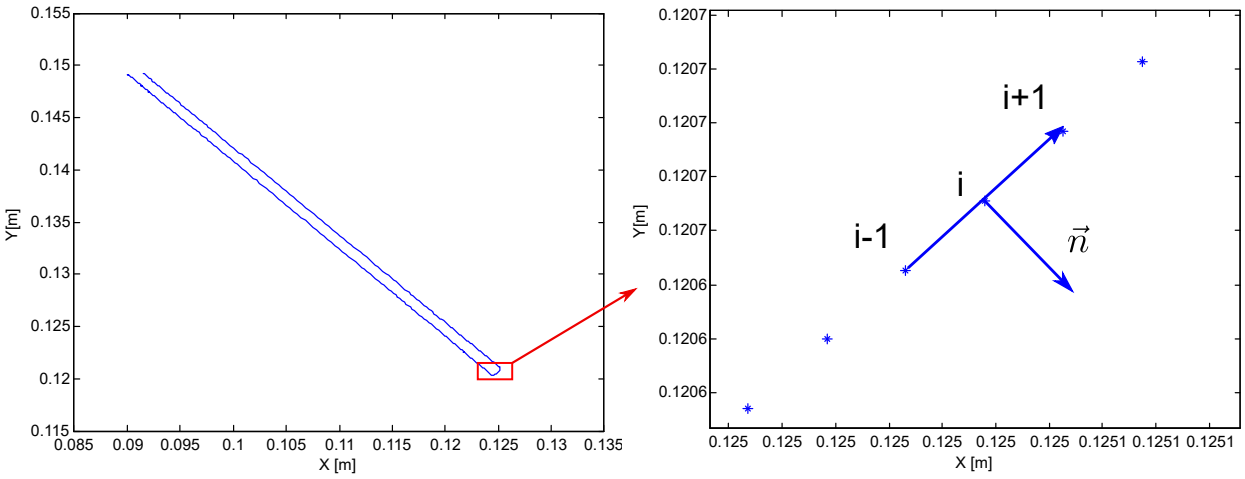

Figure 2.6: Exported Geometry of Pectoral Fin Tip (Left) and Exported Geometry of Pectoral Fin Tip Zoomed (Right) Showing the Normal Vector Used for Computations

$$\vec{F} = -\int P\vec{n}dS \tag{2.9}$$

Where $\vec{F}$ is the force vector, P is the pressure, $\vec{n}$ is the corresponding normal vector, and dS is the arc length around each point of the fin.

To quantify how much the opercular jet affects the flow, the root mean squared (RMS) difference between the pectoral fin forces generated from the baseline case (no opercular jet flow) and the case with an opercular jet flow was calculated for every parametric study value. Only the last cycle of the pectoral fin motion was considered to ensure that the flow had reached steady state. The RMS difference was calculated using Equation 2.10.

$$RMS = \sqrt{\frac{\sum_{i=1}^{n}(F_{i,baseline} - F_i)^2}{n}} \tag{2.10}$$

Where $F_{i,baseline}$ is the force generated by pectoral fin at time i for the baseline case (no opercular jet), F_i is the force generated by the pectoral fin at time i for the corresponding parametric study case, and n is the number of time steps used.

CHAPTER 3

Results

3.1 Characteristics of the Flow

The flow created by the oscillation of the pectoral fin plus flow from the opercular opening comprises of a few main flow structures. The first is the vortex shedding created at the tip of the pectoral fin when it oscillates back and forth. This is characterized by a vortex created with negative vorticity strength during the adduction (downstroke) phase and a vortex created with positive vorticity strength during the abduction (upstroke) phase, as seen in the videos in the supplemental material. Both of these vortexes dissipate as they travel downstream. As St decreases, larger vortexes are shed.

The second main flow structure is a corner flow where fluid leaves the opercular opening and follows along the pectoral fin. This flow structure can also be seen in the videos in the supplemental material.

Another important flow structure is the boundary layer that develops along the pectoral fin and boundary layer that develops on the fish body both in front of and behind the pectoral fin. As St decreases, the thickness of the boundary layer at the fin body in front (left) of the pectoral fin increases. Once St decreases to 0.1, this boundary layers creates enough vorticity to interact with the pectoral fin as well.

A final characteristic of this flow occurs between the pectoral fin and fish body. When the pectoral fin goes through its adduction phase, it squeezes fluid out of the space between the pectoral fin and fish body. On the other hand, fluid flows back into this space when the pectoral fin goes through its abduction phase. Together, all of these characteristics of this flow shows just how complex this interaction is.

3.2 Varying ΔP

Figure 3.1 shows the thrust and side slip forces created by the pectoral fin while varying ΔP. Note that t/τ refers to the period of pectoral fin motion after the simulation reaches steady state. All cases here have no swimming speed ($St = \infty$) and 0° phase difference between the pectoral fin motion and opercular opening motion.

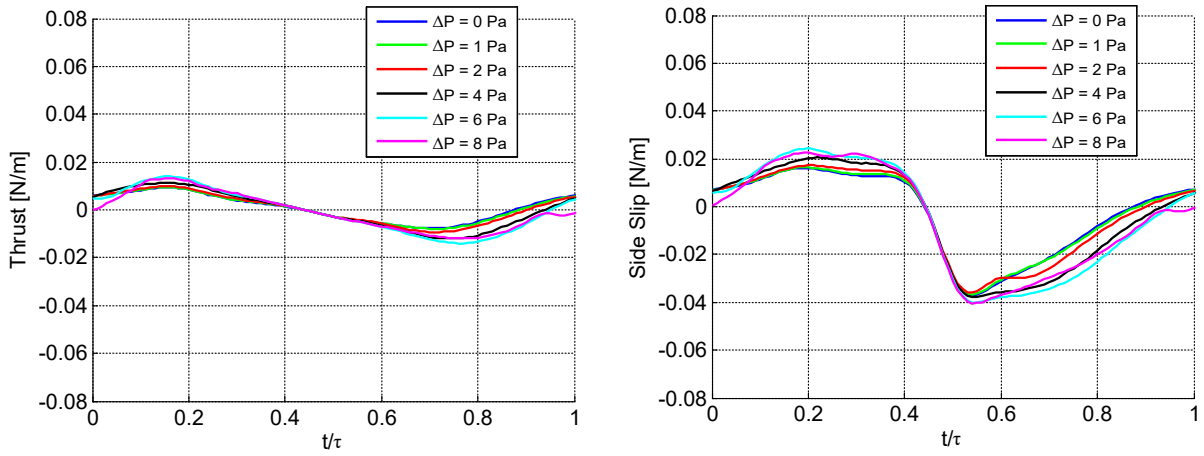

Figure 3.1: Thrust (Left) and Side Slip Forces (Right) Over 1 Pectoral Fin Movement Period, Varying ΔP

As a result, Figure 3.2 shows the RMS difference for thrust and side slip forces between the baseline case of having no opercular jet flow ($\Delta P = 0$ Pa) and the cases of varying ΔP over 1 pectoral fin movement cycle. The forces in these plots are nondimensionalized by the force from the dynamic pressure due to the fin tip velocity.

There is a linear relationship between ΔP and RMS difference of both thrust and side slip forces, as seen in Figure 3.2. Increasing ΔP by 1 Pa increases nondimensional thrust by about 1.48 and increases nondimensional side slip by about 3.4. Thus, increasing flow through the opercular opening has a larger (over 2x) effect on increasing side slip forces than it does on increasing thrust. Fish potentially can use this extra force to help them maneuver or even help them reject any side force disturbances while swimming. While a fish cannot infinitely increase this flow at any given moment, even a moderate case such as

nondimensional pressure = 98.8 (ΔP = 2 Pa) generates non-negligible forces compared to just the pectoral fin alone.

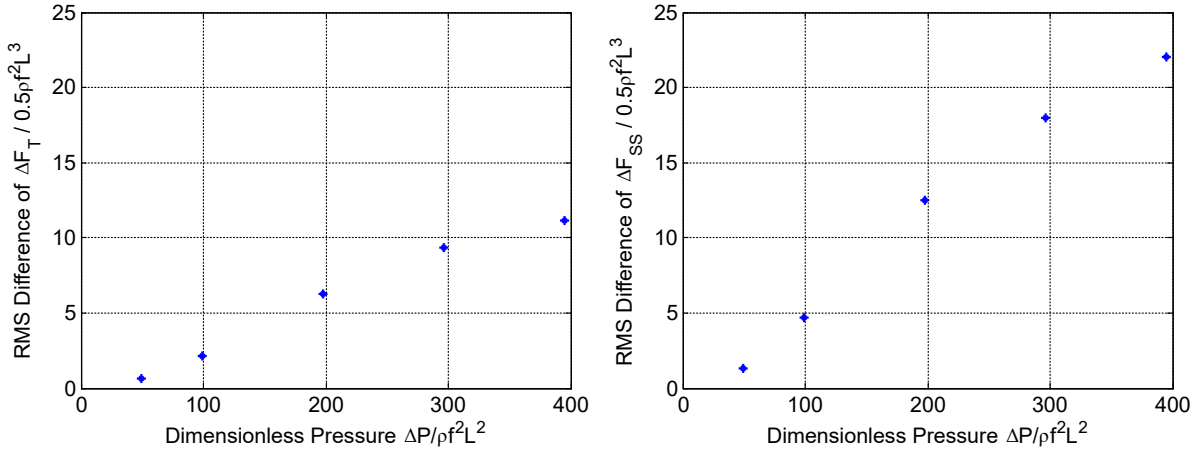

Figure 3.2: RMS Differences of Nondimensionalized Thrust (Left) and Nondimensionalized Side Slip (Right) Over 1 Pectoral Fin Movement Period, Varying ΔP

To explain the differences in each case, the pressure distribution along the outer portion of the pectoral fin was plotted at every fifth of the period over the entire period, while varying ΔP. For these plots, 0 m denotes the base of the outer portion of the pectoral fin while 0.045 m denotes the tip of the outer portion of the pectoral fin. Only the outer portion of the fin was plotted since the opercular jet only interacts with the outer portion and thus this is where differences in cases would occur. These plots are seen in Figures 3.3 and 3.4. For visualization purposes, they are plotted next to the vorticity surface plots at the same corresponding times. Similar plots can be found for the rest of the times in the cycle in the Appendix Figures A.1 and A.2.

Figures 3.3 and 3.4 show that throughout the abduction and adduction cycle, varying ΔP has a large effect on the pressure distribution along the pectoral fin, especially near the base of the fin (0 m). This is expected since the flow from the opercular opening predominantly interacts and affects the pectoral fin near its base. For example, there is some change in pressure at $t/\tau = 0.0$ near the tip of the pectoral fin (0.045 m) when ΔP increases, but this difference in pressure is not as significant as the difference in pressure near the base (0 m).

In general, this difference linearly increases as ΔP increases. It is also interesting to note that for high ΔP cases, the pressure can be higher at the base but lower at the tip compared to the smaller ΔP cases (see $t/\tau = 0$, 0.2). However, this lower pressure is not enough to offset the initial pressure increase created from the opercular opening and vastly change the thrust and side slip forces generated.

The mean force plots for these cases can also be found in Appendix Figures A.7 and A.8. The overall mean of thrust is around 0 N/m, as seen in Figure A.7. This is expected because the model fin is rigid and thus has a thrust producing phase and a drag producing phase, which roughly cancel each other out. While this simplified model is unrealistic, the trends in the RMS difference and pressure plots show that this interaction is rather complex (even for a simplified model) and can affect the forces generated by the pectoral fin.

The spatial average velocity through the opercular channel at the beginning of the pectoral fin movement cycle ($t/\tau = 0.0$) was also computed for each case, as seen in Table 3.1. This calculates the average velocity when the opercular opening is at its maximum opening area.

Table 3.1: Average Spatial Velocity Though Opercular Opening at $t/\tau = 0$

ΔP	U_{mag}	U	V
1 Pa	0.012276 m/s	0.012154 m/s	-0.0017254 m/s
2 Pa	0.022841 m/s	0.022689 m/s	-0.0026276 m/s
4 Pa	0.046665 m/s	0.046431 m/s	-0.004617 m/s
6 Pa	0.064874 m/s	0.064497 m/s	-0.0069162 m/s
8 Pa	0.078085 m/s	0.077534 m/s	-0.0092088 m/s

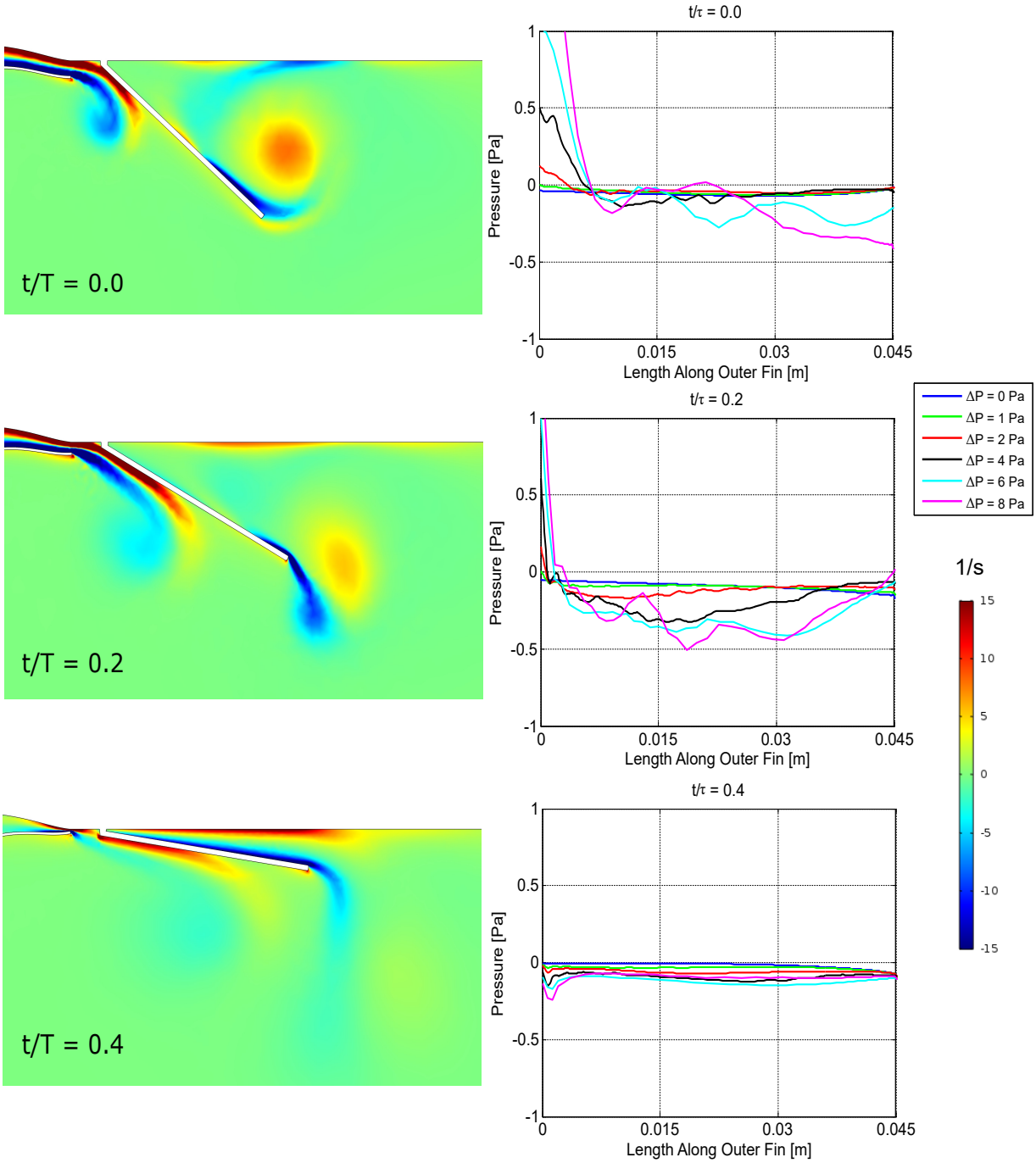

Figure 3.3: Vorticity Surface Plots (Left) and Pressure Distribution Plots (Right) at Every Fifth of the Pectoral Fin Movement Period from t/τ= 0.0 to t/τ= 0.4, Varying ΔP. Vorticity Surface Plots are for ΔP = 2 Pa, 0° Phase Difference, St = ∞

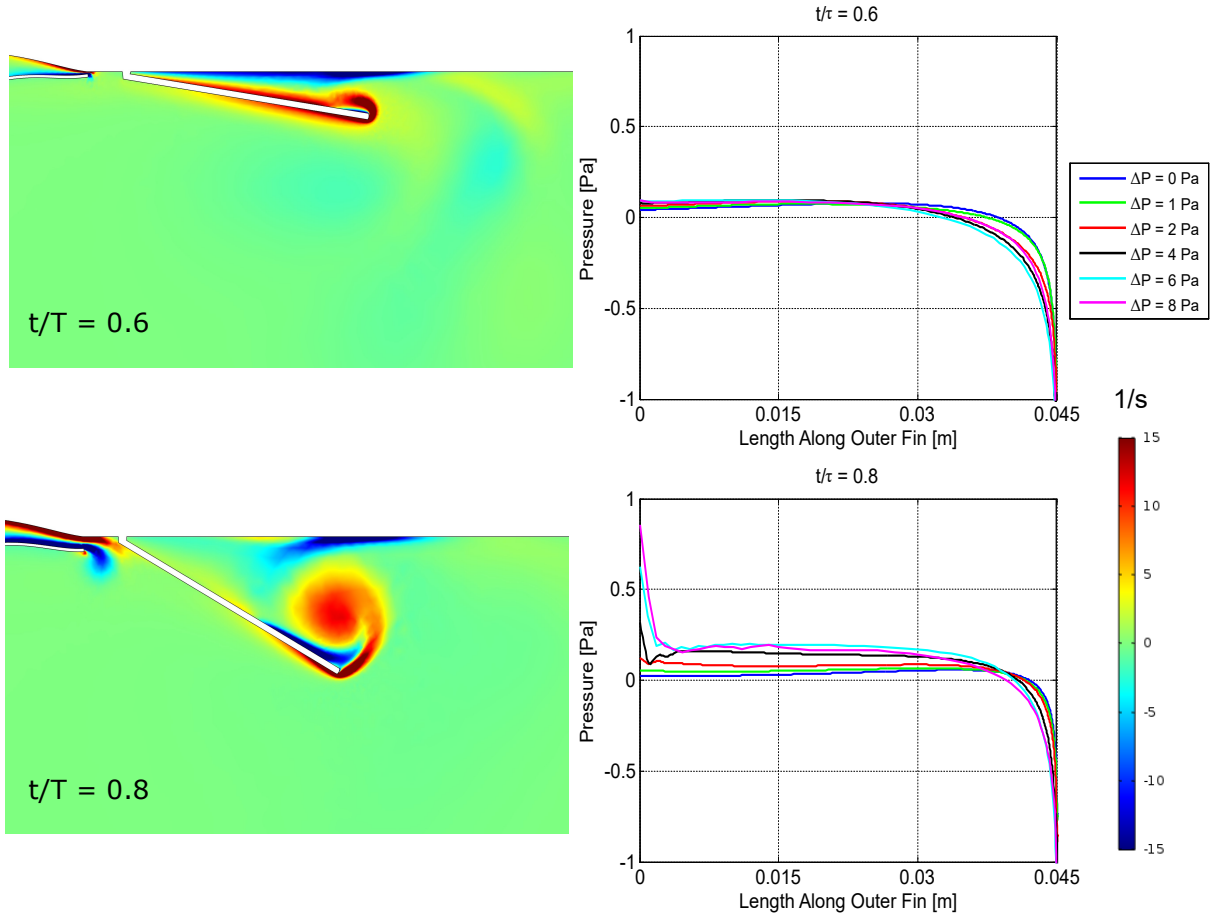

Figure 3.4: Vorticity Surface Plots (Left) and Pressure Distribution Plots (Right) at Every Fifth of the Pectoral Fin Movement Period from t/τ= 0.6 to t/τ= 0.8, Varying ΔP. Vorticity Surface Plots are for ΔP = 2 Pa, 0° Phase Difference, St = ∞

3.3 Varying Phase Difference

Similarly, the same procedure is done for varying phase difference between the pectoral fin and opercular opening cycles. For all of these cases, ΔP = 2 Pa and St = ∞. The baseline case is once again taken as the no opercular jet flow case (ΔP = 0 Pa) with 0° phase difference and St = ∞. The thrust and side slip plots can be found in Figure 3.5 while the RMS difference plots of thrust and side slip can be found in Figure 3.6.

There is a relatively minor oscillatory trend in RMS difference of thrust and side slip

forces when increasing the phase difference between the pectoral fin and opercular opening motions, as seen in Figure 3.6. This difference is fairly small compared to the difference in forces while varying ΔP. In varying phase difference, the smallest difference in side slip from the baseline case occurs at -180 degrees phase difference while the largest difference occurs at 45 degrees phase difference. The nondimensional side slip difference between these two cases is 2.47. This difference is equivalent to a ΔP of 0.73 Pa. Meanwhile, the largest difference in thrust from the baseline occurs at -180 degrees phase difference while the smallest difference occurs at -45 degrees phase difference. The nondimensional thrust difference between these two cases is 0.77, which is equivalent to a ΔP of 0.52 Pa. The minor difference between changing phase difference is likely the result of the corner flow from the opercular opening lingering along the pectoral fin at all phase differences, which washes out any difference in pressure that would occur.

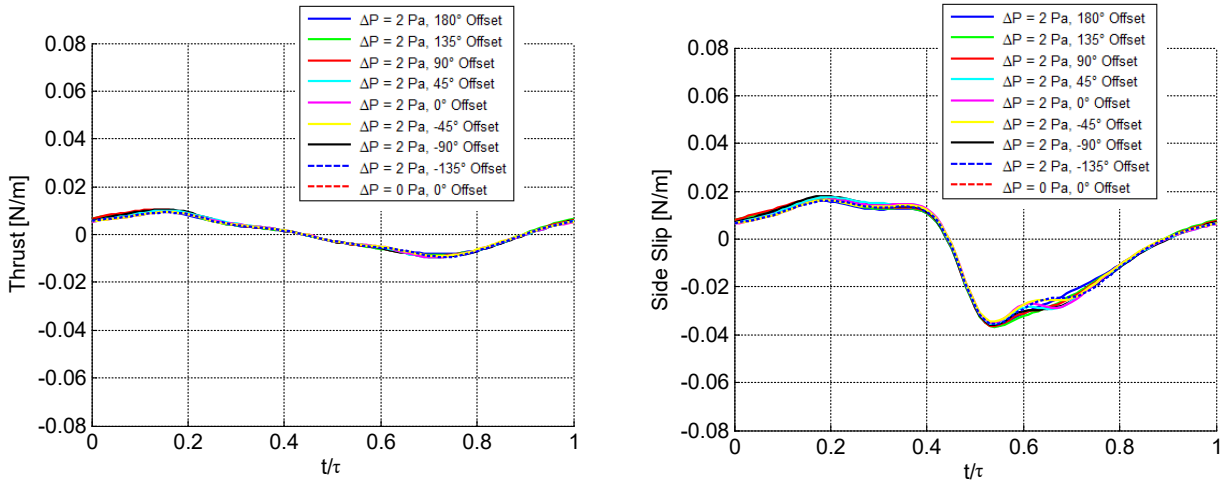

Figure 3.5: Thrust (Left) and Side Slip Forces (Right) Over 1 Pectoral Fin Movement Period, Varying Phase Difference

The pressure distribution plots along with the corresponding vorticity surface plots can be seen in Figures 3.7 and 3.8. These plots show that at different times in the pectoral fin movement cycle, the biggest changes in pressure (compared to the case with $\Delta P = 0$ Pa and 0° phase difference) occur at different phase differences. For example, at $t/\tau = 0.0$, the 90 degree phase difference case has the largest pressure near the fin base while at t/τ

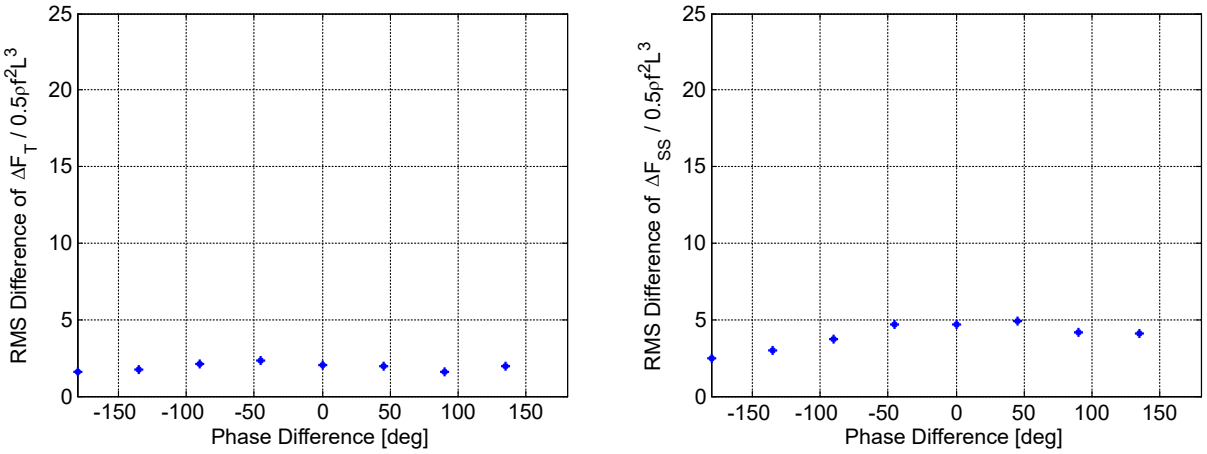

Figure 3.6: RMS Differences of Nondimensionalized Thrust (Left) and Nondimensionalized Side Slip (Right) Over 1 Pectoral Fin Movement Period, Varying Phase Difference

= 0.4, the 0 degrees phase difference case has the largest pressure (in magnitude) near the fin base. This is expected since the flow from the opercular jet interacts with the pectoral fin at different times for different phase differences. The initial differences at the base are rather minimal compared to the similarity in pressure distribution toward the tip such that the overall forces generated from this pressure distribution is similar for all cases, as seen in Figures 3.7 and 3.8. The plots corresponding to the rest of the times in the cycle can be found in the Appendix Figures A.3 and A.4.

The mean force plots for these cases can also be found in Appendix Figures A.9 and A.10. As expected, there is little deviation in mean thrust and side slip forces for all of the various phase difference cases.

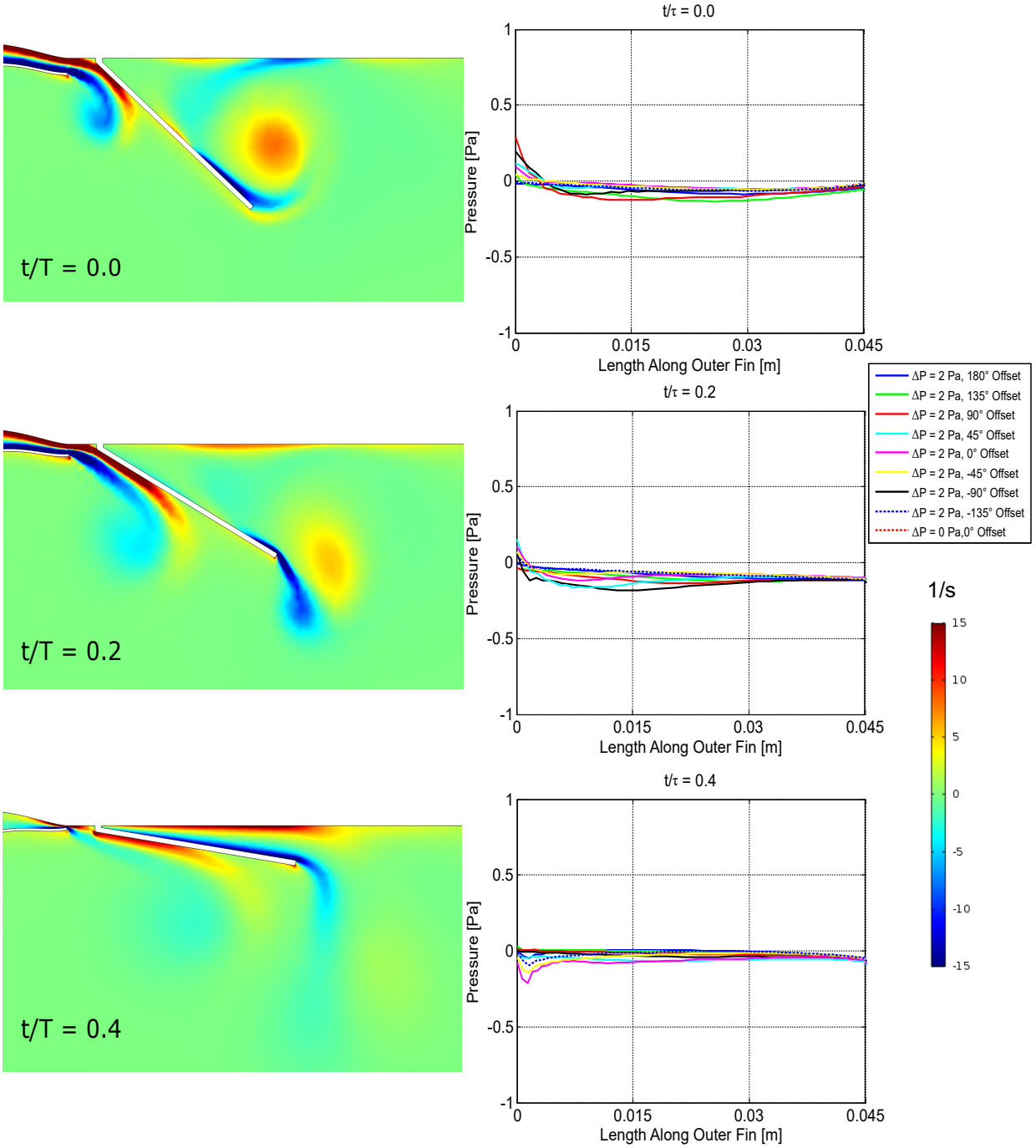

Figure 3.7: Vorticity Surface Plots (Left) and Pressure Distribution Plots (Right) at Every Fifth of the Pectoral Fin Movement Period from t/τ= 0.0 to t/τ= 0.4, Varying Phase Difference. Vorticity Surface Plots are for ΔP = 2 Pa, 0° Phase Difference, St = ∞

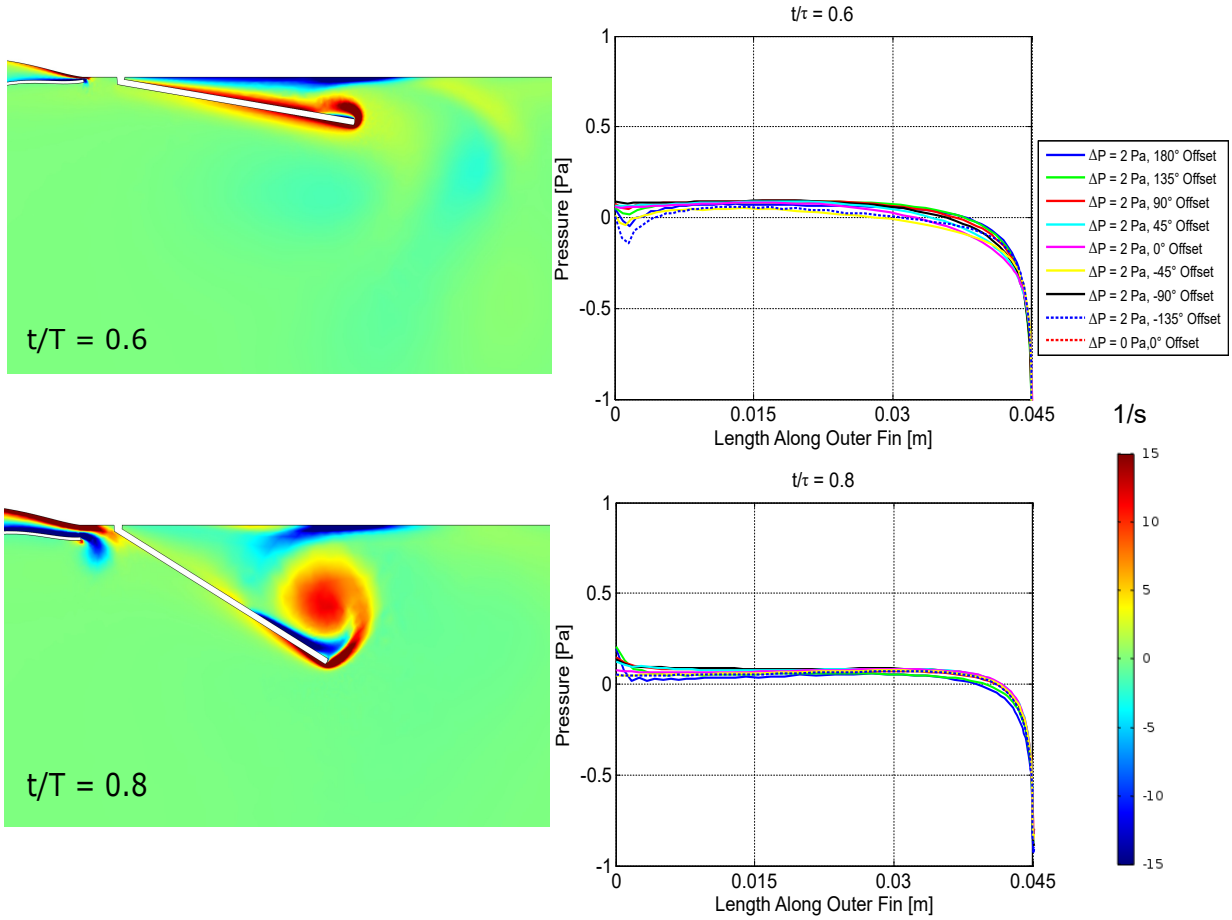

Figure 3.8: Vorticity Surface Plots (Left) and Pressure Distribution Plots (Right) at Every Fifth of the Pectoral Fin Movement Period from t/τ= 0.6 to t/τ= 0.8, Varying Phase Difference. Vorticity Surface Plots are for ΔP = 2 Pa, 0° Phase Difference, St = ∞

3.4 Varying Strouhal Number

Finally, the same procedure is done for varying Strouhal Number. All of these cases have 0° phase difference and ΔP = 2 Pa. For each Strouhal Number, the baseline case is taken as the no opercular flow case (ΔP = 0 Pa) with 0° phase difference at the same corresponding Strouhal Number. The thrust and side slip plots can be found in Figure 3.9 while the RMS difference plots of thrust and side slip can be found in Figure 3.10. Note that as St decreases, there is more drag created by the fin.

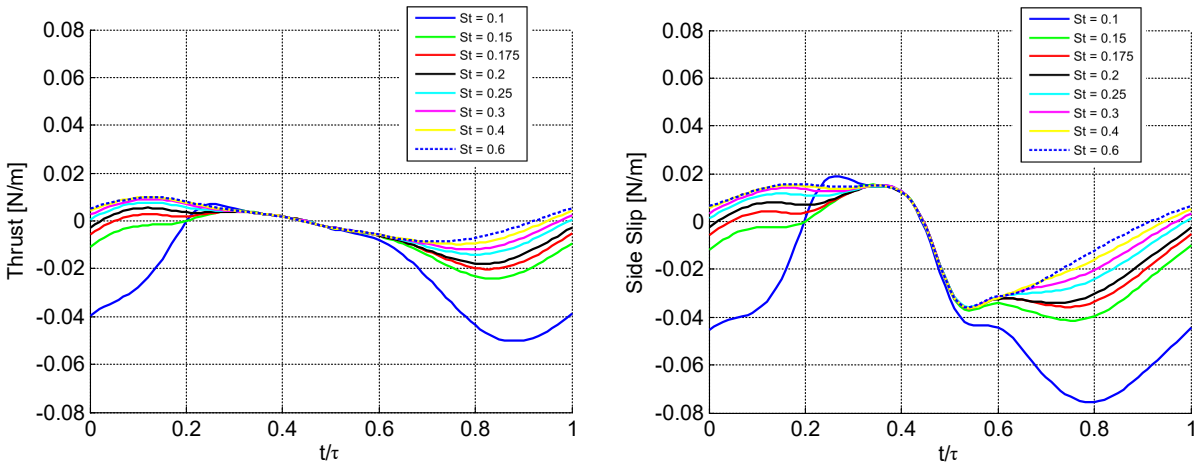

Figure 3.9: Thrust (Left) and Side Slip Forces (Right) Over 1 Pectoral Fin Movement Period, Varying St

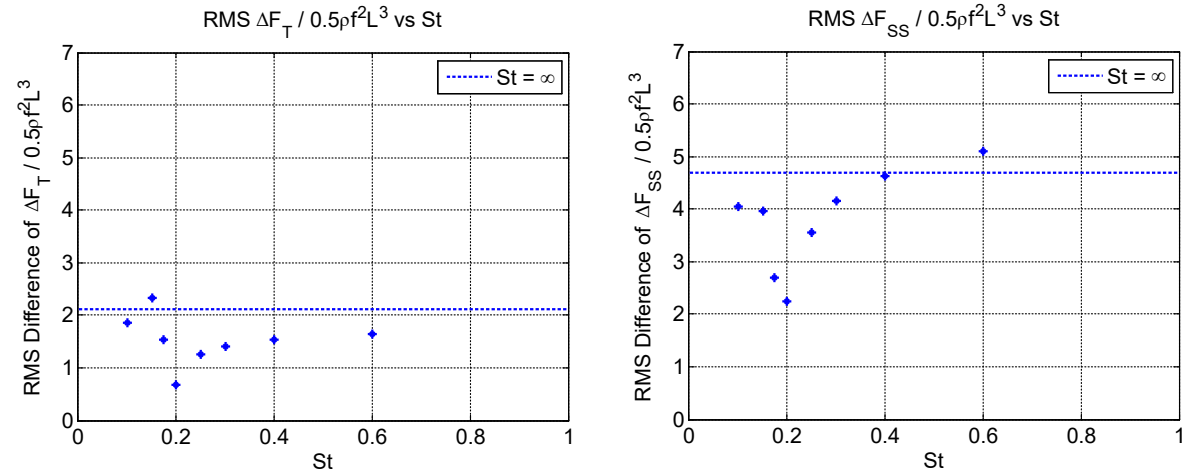

Figure 3.10: RMS Differences of Nondimensionalized Thurst (Left) and Nondimensionalized Side Slip (Right) Over 1 Pectoral Fin Movement Period, Varying St

From varying St, there is an interesting nonlinear trend in the RMS difference, as seen in Figure 3.10. There are 2 sections that have different trends. For the higher St cases (St > 0.2), the RMS difference increases then levels off as St increases. However, for St < 0.2, there is initially a substantial RMS difference, and then it drops to a minimum at St $= 0.2$. This minimum occurs when the ratio between the swimming speed and the average spatial

velocity through the opercular opening is closest to unity, as seen in Table 3.2. When this ratio is at unity, the opercular jet does not add or subtract to the freestream flow and thus is similar to the baseline case of having a freestream velocity but no jet flow. When this ratio gets further away from unity (higher or lower St), the opercular jet either increases or decreases the flow near the opercular opening compared to the baseline case. This creates a larger RMS difference since RMS difference measures the magnitude of the difference and not the sign.

The pressure distribution plots along with the corresponding vorticity surface plots can be found in Figures 3.11 and 3.12. Decreasing St tends to increase the pressure at the base of the fin, but decrease the pressure at the tip of the fin. In general, the St cases have very similar trends in the pressure distribution, with a more dramatic change (though still the same trend) in the St = 0.1 case. This is probably due to the fact that the boundary layer from the fish body in front of the pectoral fin is large enough at St = 0.1 that it now interacts with the pectoral fin itself. Regardless, it is important to note that St does in fact have an affect on the analysis of these flows. The plots corresponding to the rest of the times in the cycle can be found in Appendix Figures A.5 and A.6.

Table 3.2: Ratio of Swimming Velocity for Given St to Average Spatial Velocity Through Opercular Opening at $\Delta P = 2$ Pa

St	U_{swim}/U_{mag} at $\Delta P = 2$ Pa
0.1	1.970
0.15	1.313
0.175	1.125
0.2	0.985
0.25	0.788
0.3	0.657
0.4	0.493
0.6	0.328

The mean force plots for these cases can also be found in Appendix Figures A.11 and A.12. The mean thrust decreases and then levels off as St increases, as seen in Figure A.11. This is expected since lower St means the fish can swim farther with each stroke.

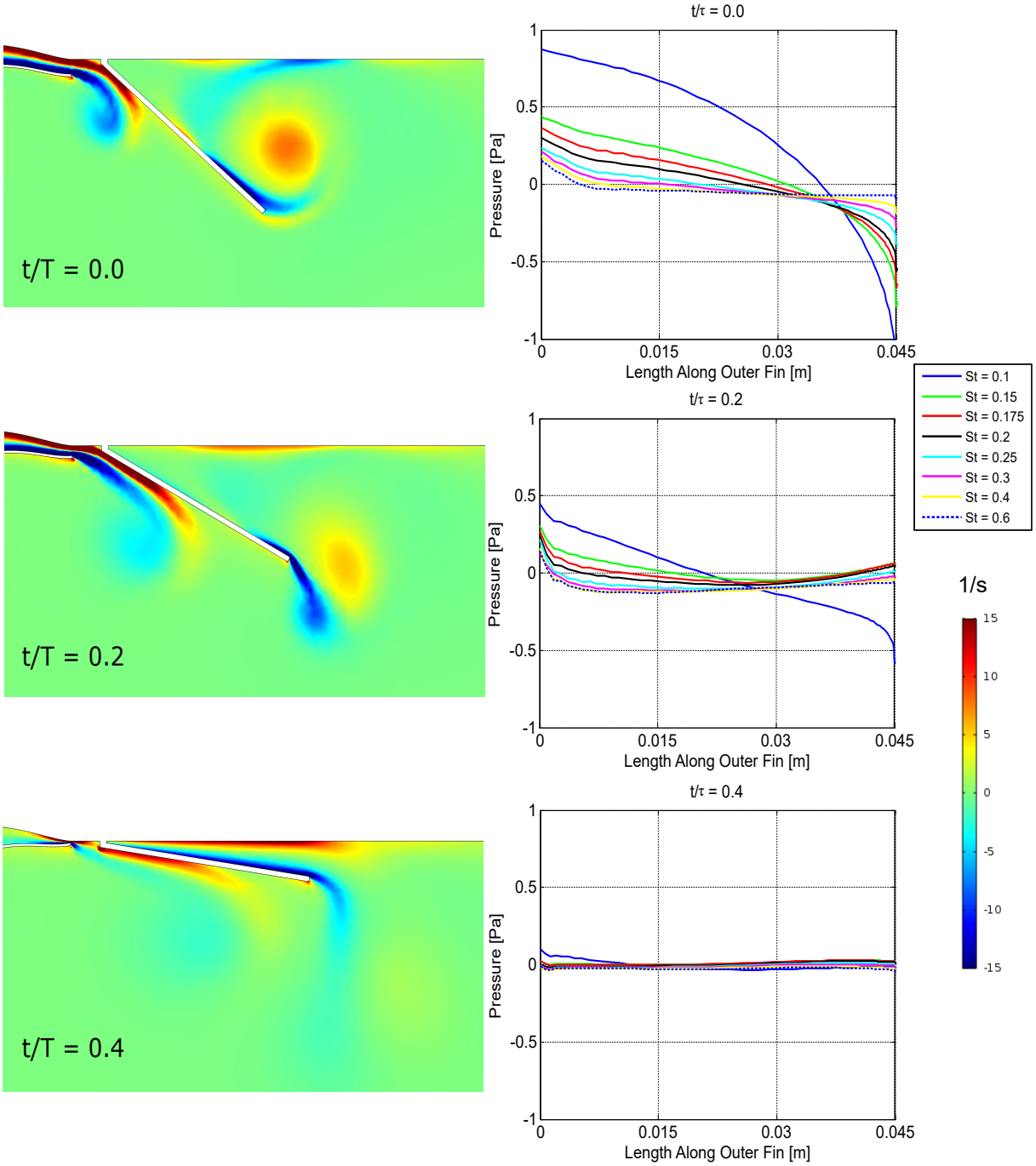

Figure 3.11: Vorticity Surface Plots (Left) and Pressure Distribution Plots (Right) at Every Fifth of the Pectoral Fin Movement Period from t/τ= 0.0 to t/τ= 0.4, Varying St. Vorticity Surface Plots are for $\Delta P = 2$ Pa, 0° Phase Difference, St = ∞

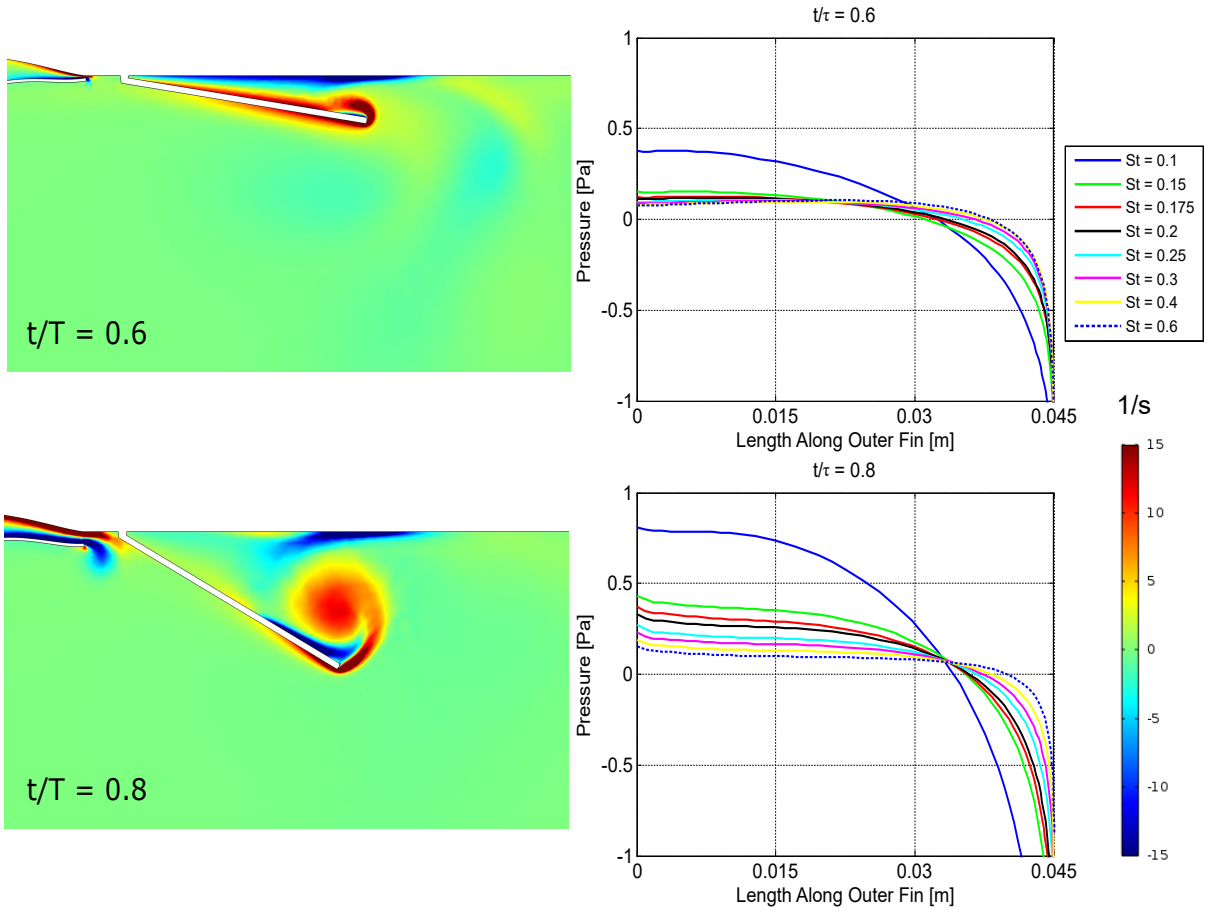

Figure 3.12: Vorticity Surface Plots (Left) and Pressure Distribution Plots (Right) at Every Fifth of the Pectoral Fin Movement Period from t/τ= 0.6 to t/τ= 0.8, Varying St. Vorticity Surface Plots are for $\Delta P = 2$ Pa, 0° Phase Difference, St = ∞

CHAPTER 4

Discussion, Conclusions, and Future Work

In conclusion, we modeled and simulated a 2D rigid labriform-swimming fish with respiratory flows and did a parametric study varying key parameters for labriform-swimming fish (ΔP, phase, and St). We found that the flow from the opecular opening due to respiration creates important and complex flow structures for labriform-swimming fish. We compared the thrust and side slip forces generated for each parametric study case and found that the flow from the opercular opening can have a significant effect on the forces generated.

In particular, increasing the flow through the opercular opening by varying ΔP affected thrust but more significantly affected the side slip forces, which are important for fish maneuverability. Varying phase difference between the opercular opening and pectoral fin motions did not significantly affect either thrust or side slip forces compared to varying ΔP. Finally, varying St created two sections where respiratory flows affected the thrust and side slip forces differently. Above St = 0.2, increasing St increased the RMS difference on thrust and side slip forces until it plateaued at St = ∞. Below St = 0.2, decreasing St also increased the RMS difference. However, there is a minimum RMS difference at St = 0.2 due to the swimming speed having roughly the same order of magnitude as the opercular jet flow speed at St = 0.2. The RMS difference once again showed that varying St is more significant to side slip than thrust. This shows that while fish can potentially use respiratory flows to swim faster, they are more likely to use these flows to help them turn or stabilize themselves from any outside disturbances.

Overall, this study has shown that the hydrodynamic interaction between respiratory flows and flows from the pectoral fin motion can have a significant effect on the thrust and side slip forces generated by labriform-swimming fish, even for a simplified model. While

this is a first look into this interaction, this study can be made more realistic and accurate in the future by adding the following:

- A flexible/deformable fin and fluid-structure interaction solver (more realistic motion of the fin and opercular opening)
- 3D capability
- Adding more values for the parametric sweep

APPENDIX A

Description of Supplemental Material and Extra Plots

A.1 Description of Supplemental Material

All of the videos in the supplemental material are of vorticity and have $\Delta P = 2$ Pa and 0° phase difference. The vorticity ranges from -15 1/s (blue) to 15 1/s (red). The pectoral fin and opercular opening both oscillate at a frequency of 0.1 Hz. The video is played at 2x speed over 3 periods of pectoral fin motion. The opercular opening motion is delayed until it is in phase with the pectoral fin motion. The differences in videos are as follows:

- VortStInf.avi has St = ∞
- VortSt3.avi has St = 0.3
- VortSt1.avi has St = 0.1

A.2 Extra Vorticity and Pressure Plots

The extra plots are on the next few pages due to size constraints.

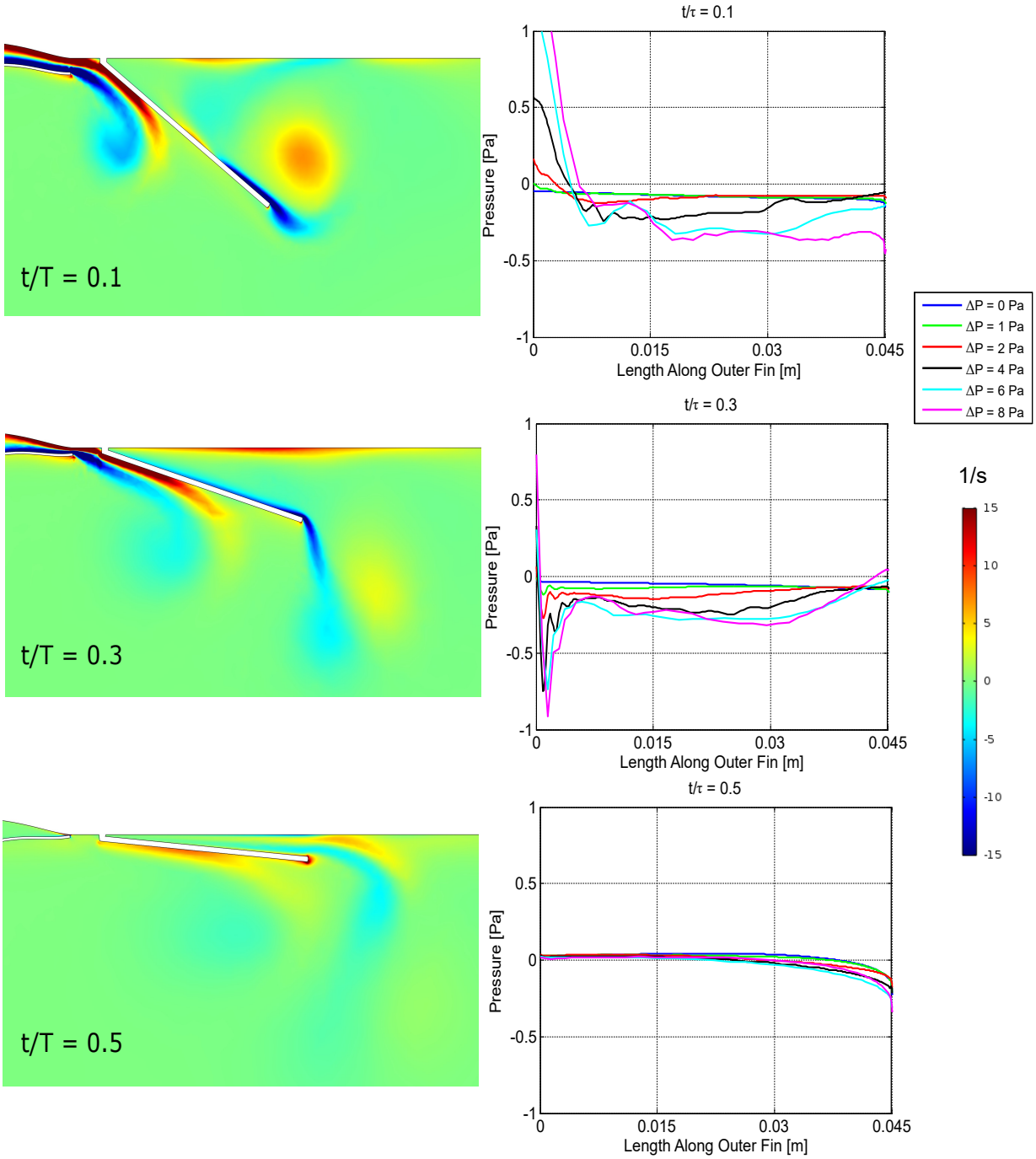

Figure A.1: Vorticity Surface Plots (Left) and Pressure Distribution Plots (Right) at Every Fifth of the Pectoral Fin Movement Period from t/τ= 0.1 to t/τ= 0.5, Varying ΔP. Vorticity Surface Plots are for ΔP = 2 Pa, 0° Phase Difference, St = ∞

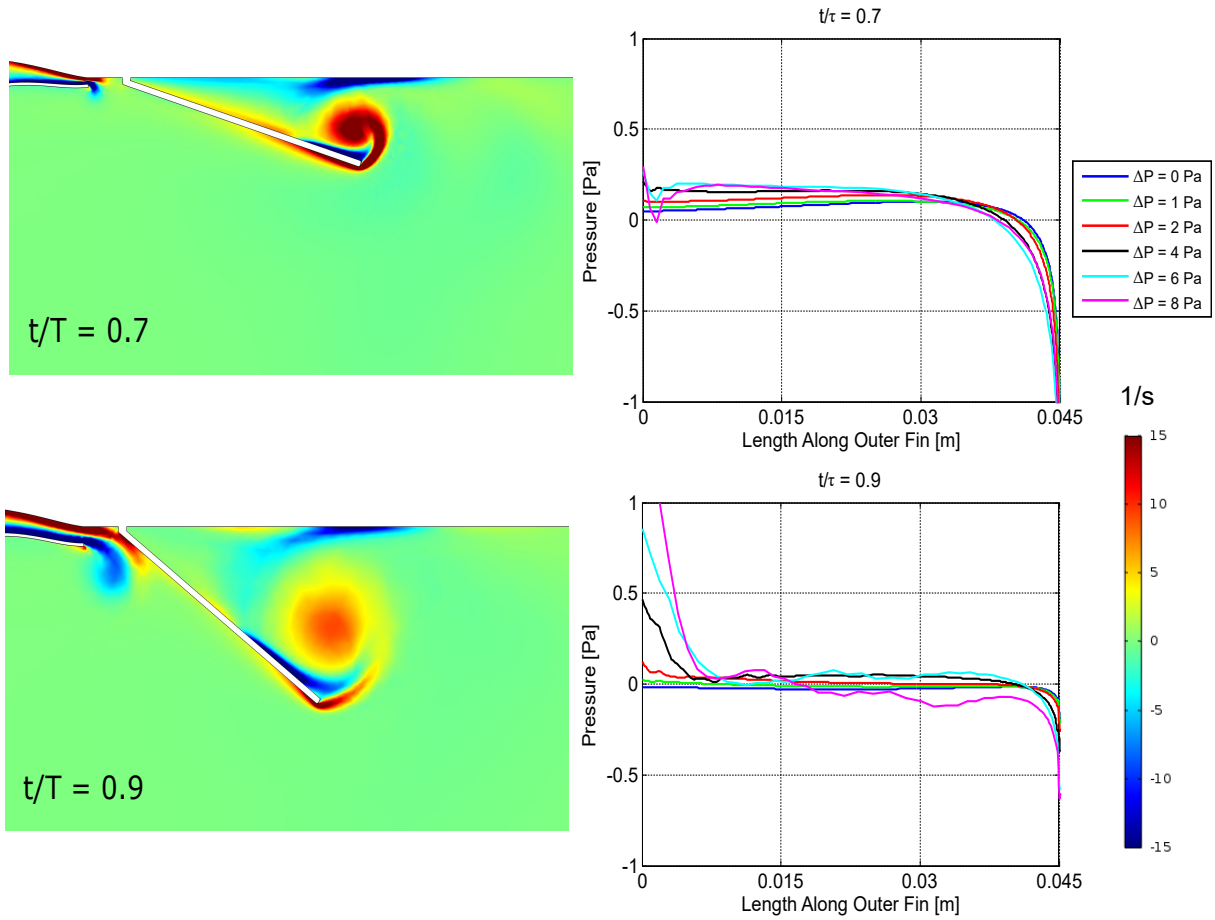

Figure A.2: Vorticity Surface Plots (Left) and Pressure Distribution Plots (Right) at Every Fifth of the Pectoral Fin Movement Period from t/τ= 0.7 to t/τ= 0.9, Varying ΔP. Vorticity Surface Plots are for ΔP = 2 Pa, 0° Phase Difference, St = ∞

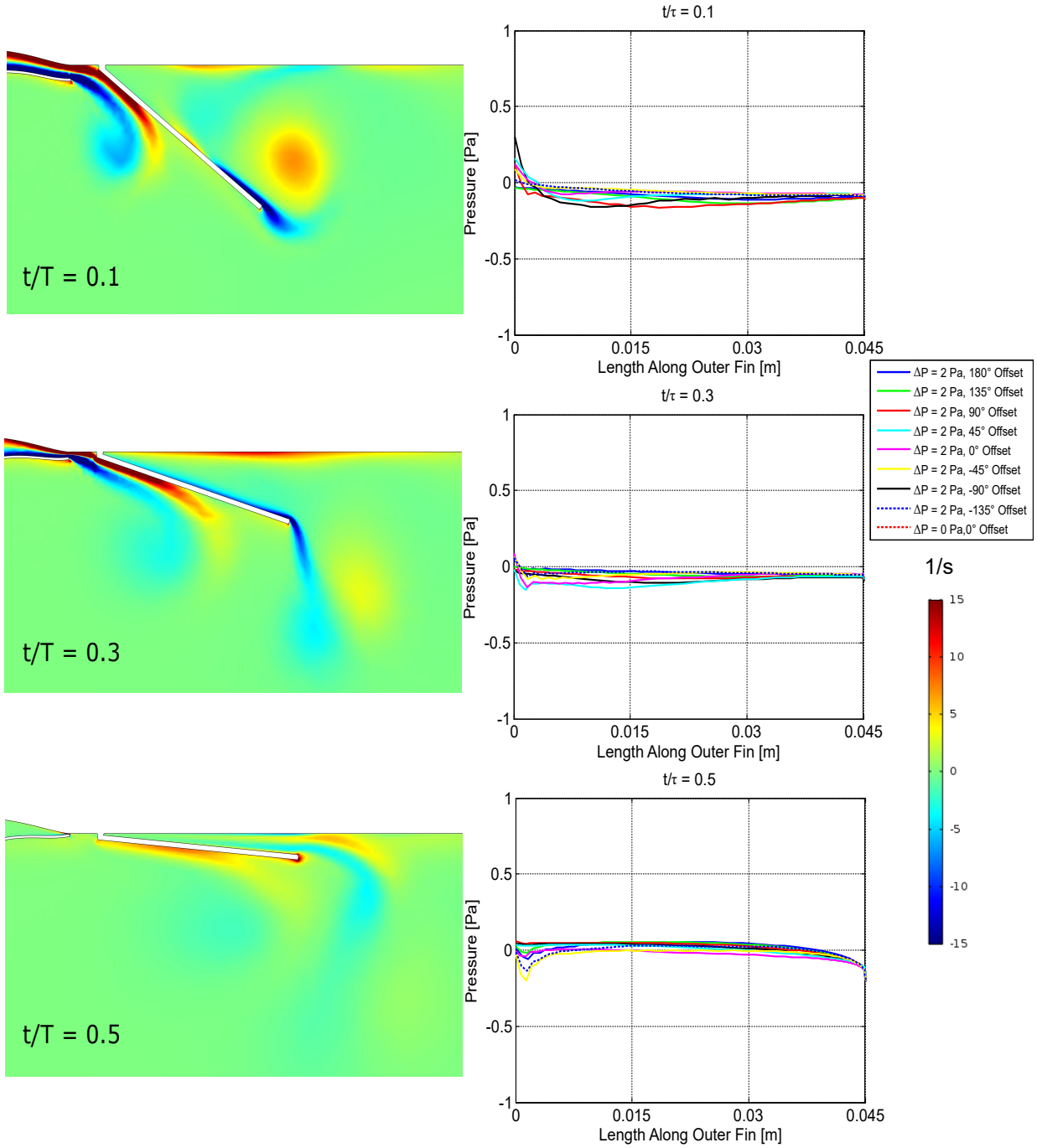

Figure A.3: Vorticity Surface Plots (Left) and Pressure Distribution Plots (Right) at Every Fifth of the Pectoral Fin Movement Period from t/τ= 0.1 to t/τ= 0.5, Varying Phase Difference. Vorticity Surface Plots are for $\Delta P = 2$ Pa, 0° Phase Difference, St = ∞

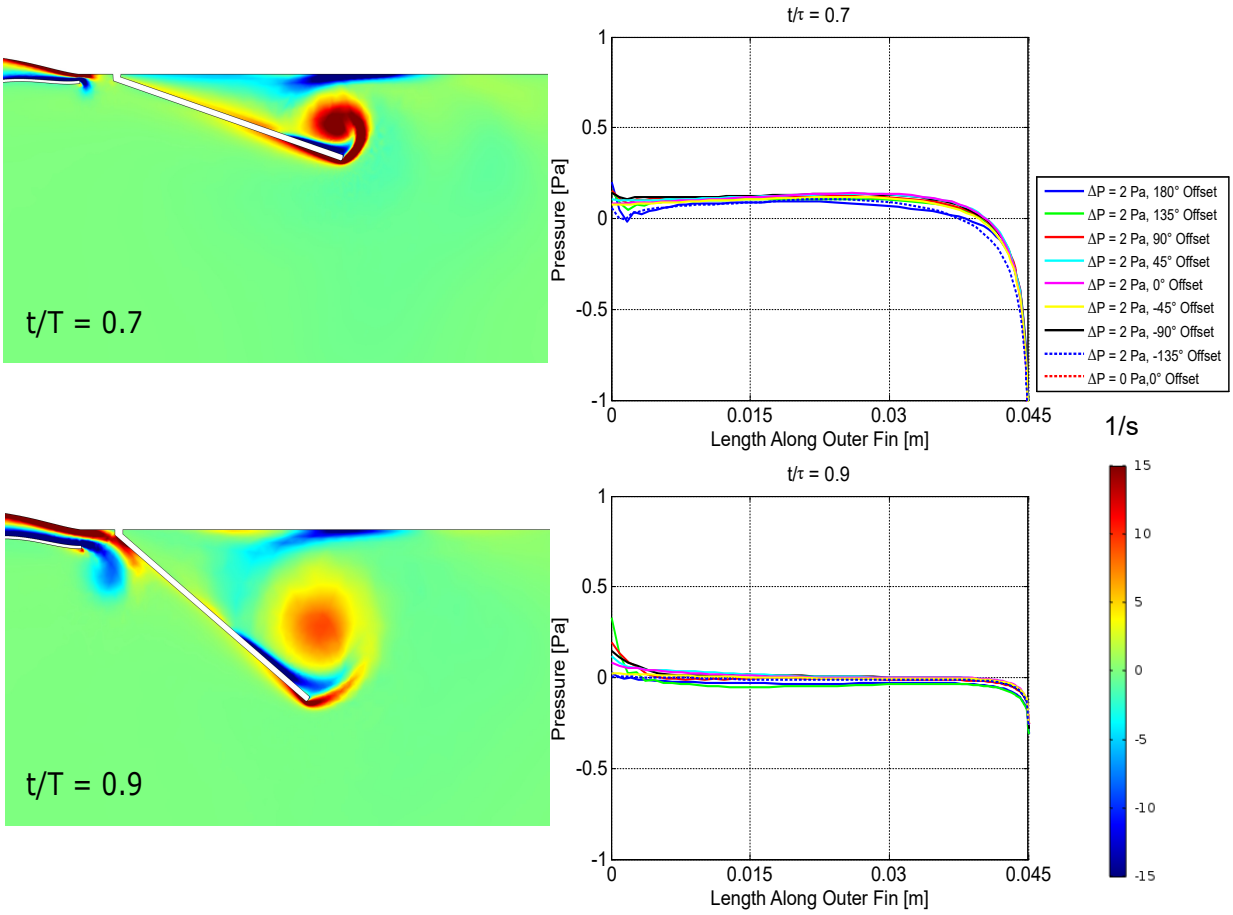

Figure A.4: Vorticity Surface Plots (Left) and Pressure Distribution Plots (Right) at Every Fifth of the Pectoral Fin Movement Period from t/τ= 0.7 to t/τ= 0.9, Varying Phase Difference. Vorticity Surface Plots are for $\Delta P = 2$ Pa, 0° Phase Difference, St $= \infty$

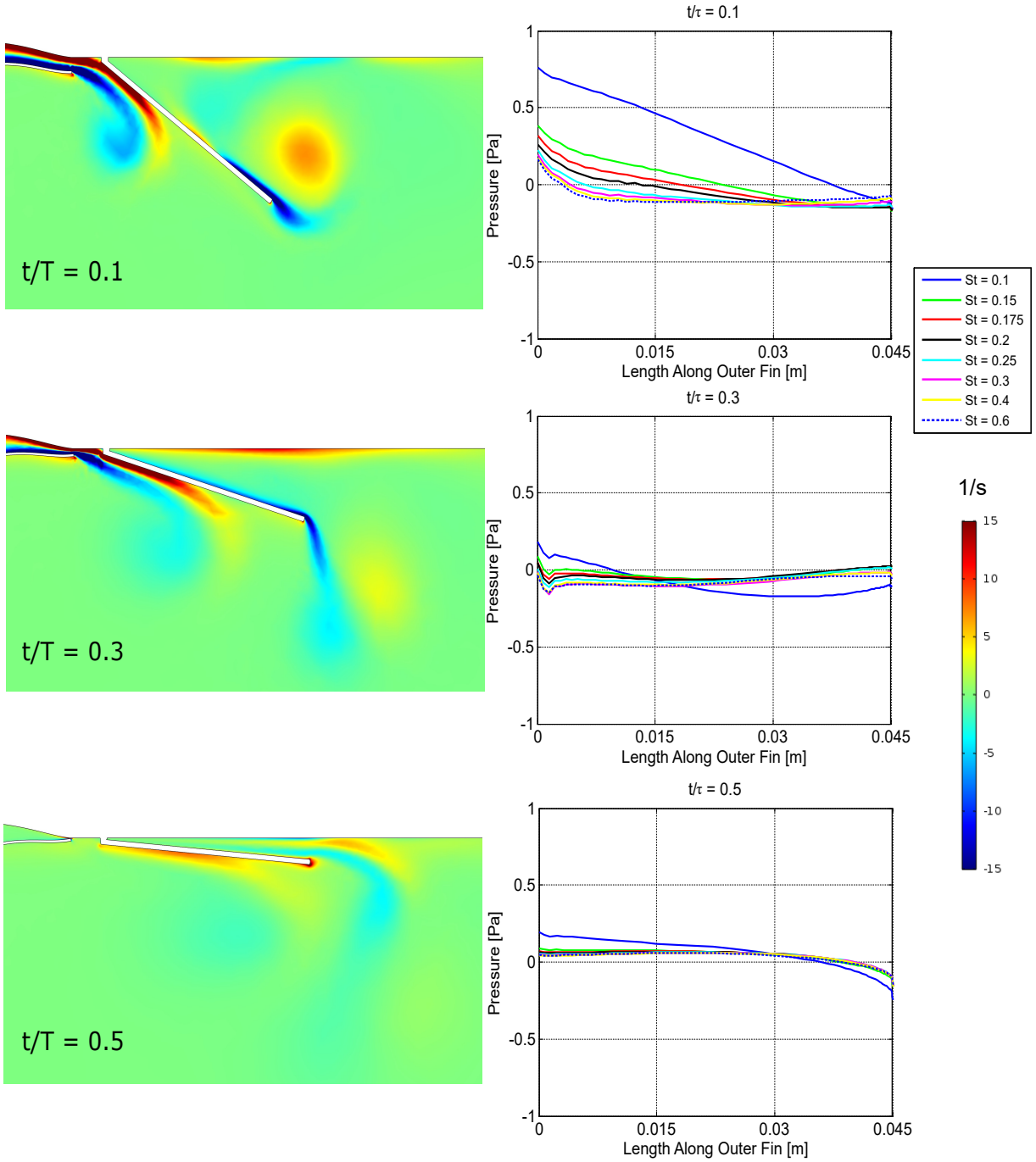

Figure A.5: Vorticity Surface Plots (Left) and Pressure Distribution Plots (Right) at Every Fifth of the Pectoral Fin Movement Period from t/τ= 0.1 to t/τ= 0.5, Varying St. Vorticity Surface Plots are for $\Delta P = 2$ Pa, 0° Phase Difference, St = ∞

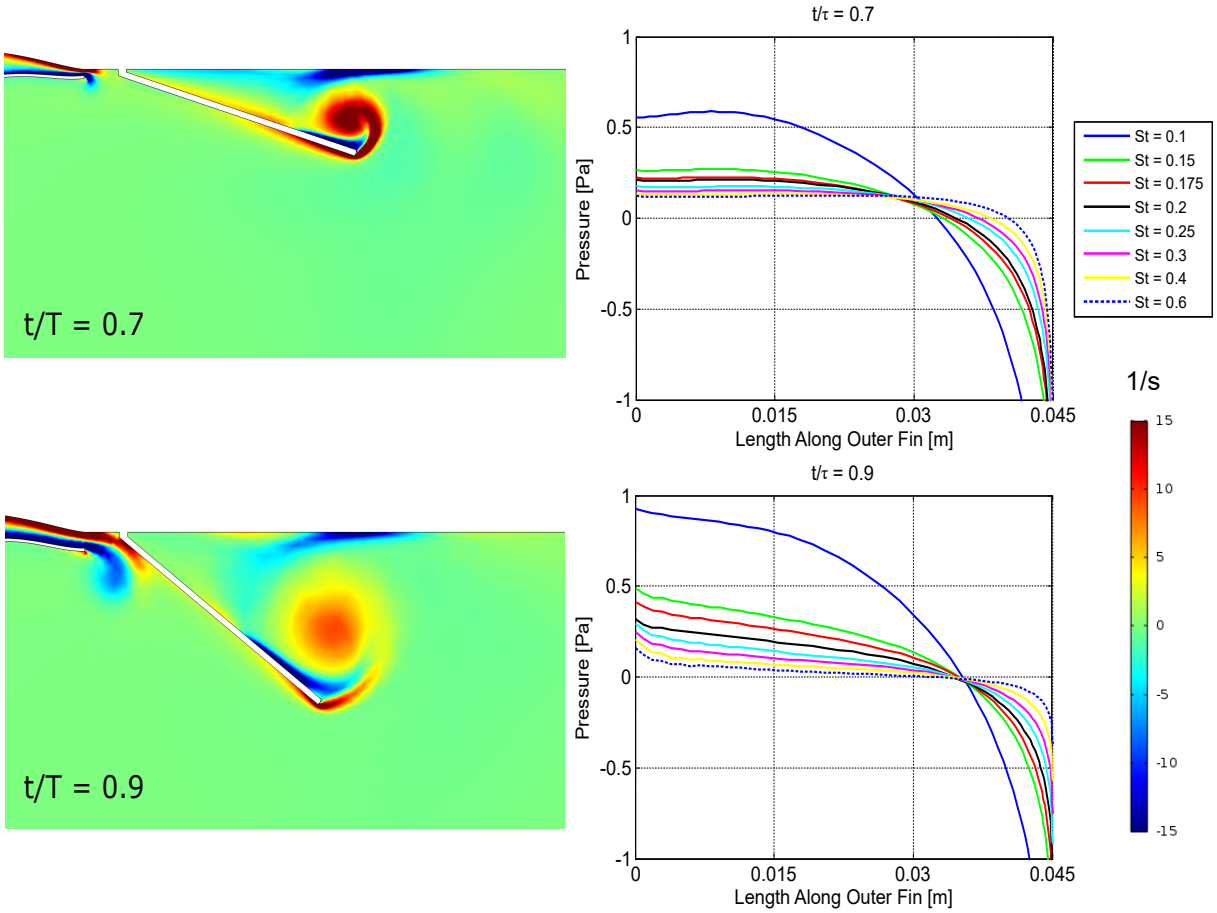

Figure A.6: Vorticity Surface Plots (Left) and Pressure Distribution Plots (Right) at Every Fifth of the Pectoral Fin Movement Period from t/τ= 0.7 to t/τ= 0.9, Varying St. Vorticity Surface Plots are for $\Delta P = 2$ Pa, 0° Phase Difference, St = ∞

A.3 Mean Force Plots

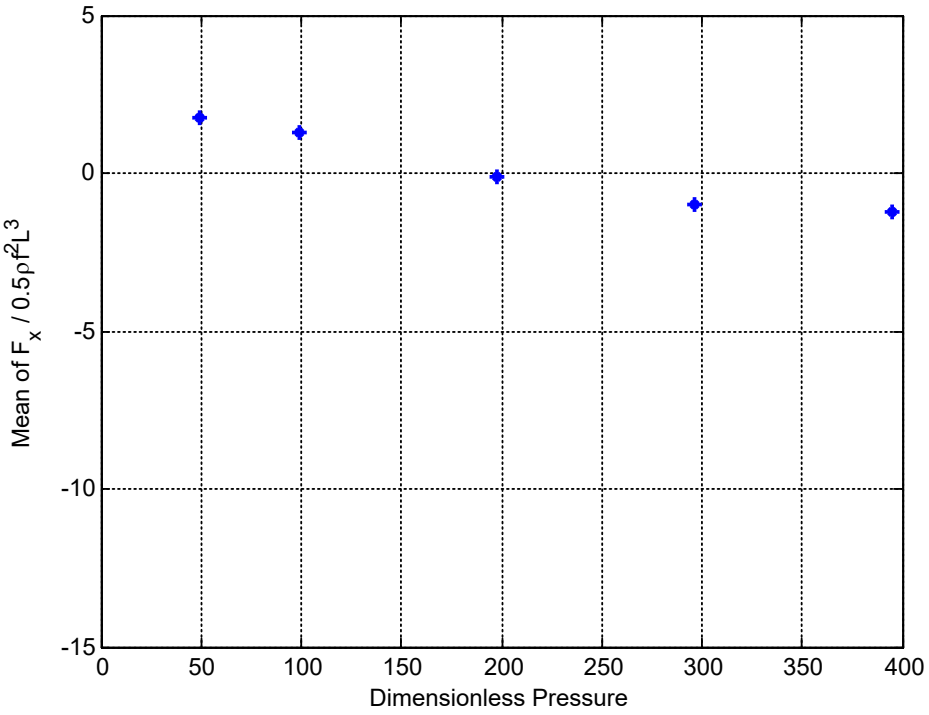

Figure A.7: Mean Dimensionless Force in x Direction vs. Dimensionless Pressure

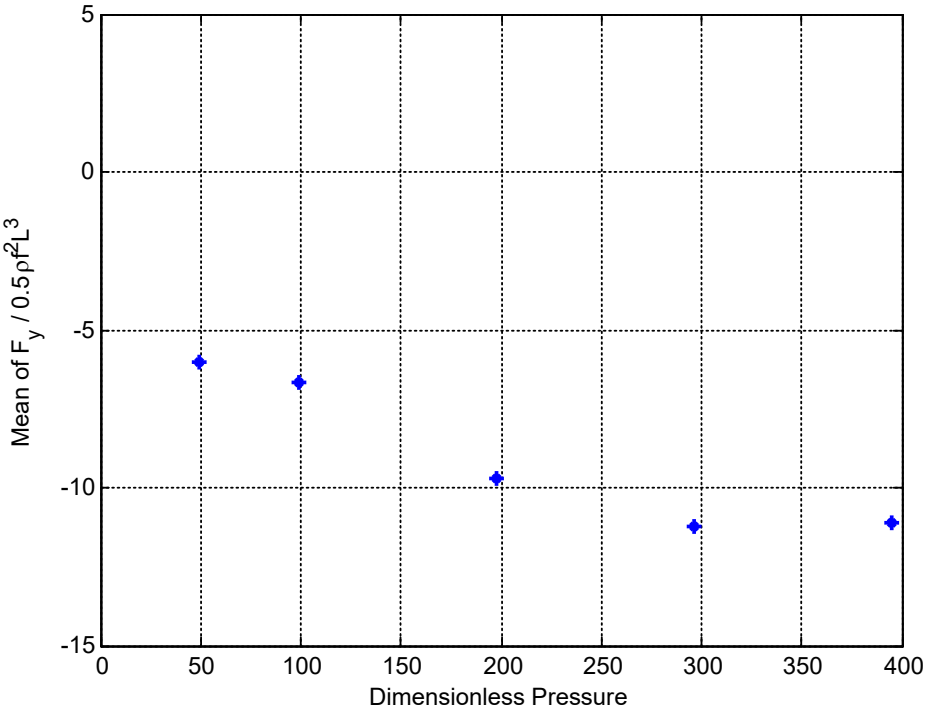

Figure A.8: Mean Dimensionless Side Slip vs. Dimensionless Pressure

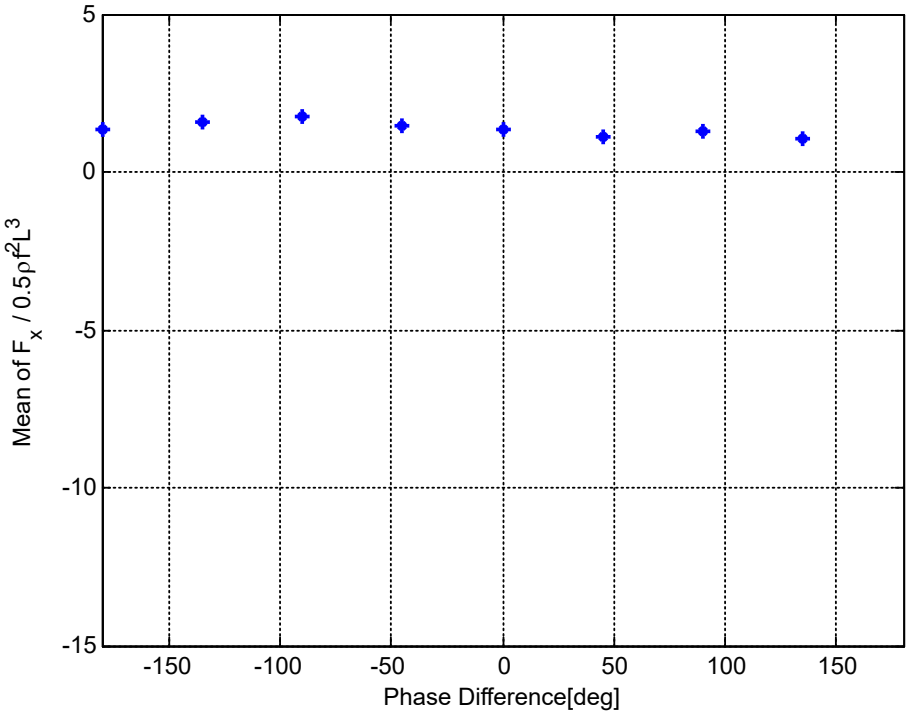

Figure A.9: Mean Dimensionless Force in x Direction vs. Phase Difference

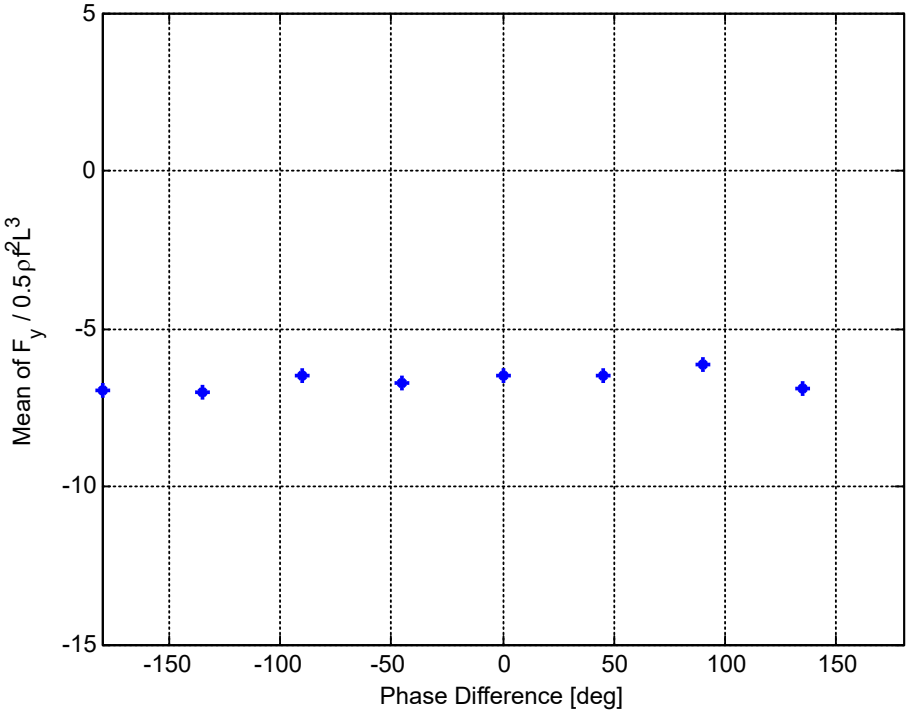

Figure A.10: Mean Dimensionless Side Slip vs. Phase Difference

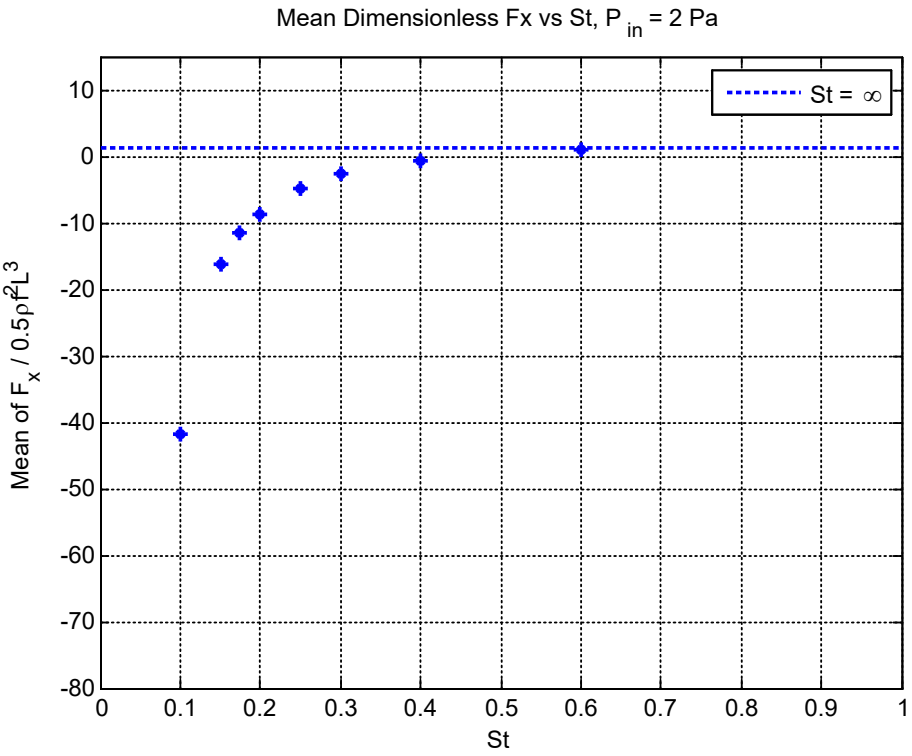

Figure A.11: Mean Dimensionless Force in x Direction vs. St

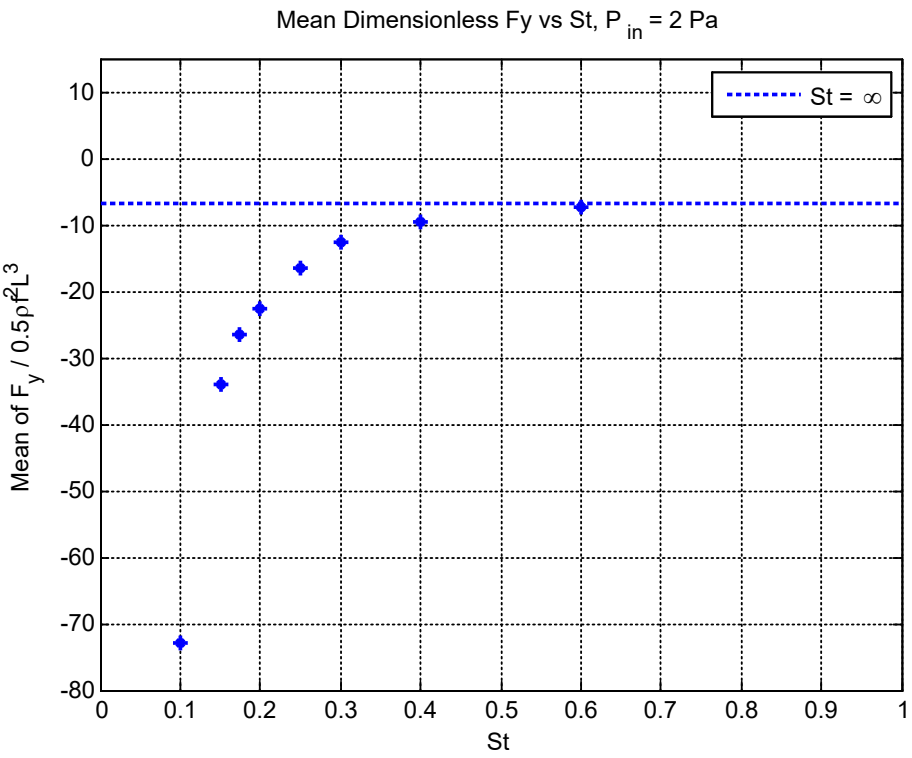

Figure A.12: Mean Dimensionless Side Slip vs. St

REFERENCES

[1] Bozkurttas, M., Mittal, R., Dong, H., Lauder, G.V. and Madden, P. (2009). Low-dimensional models and performance scaling of a highly deformable fish pectoral fin. *J. Fluid Mech.* **631**, 311-342.

[2] Dong, H., Bozkurttas, M., Mittal, R., Madden, P. and Lauder, G.V. (2010). Computational modeling and analysis of the hydrodynamics of a highly deformable fish pectoral fin. *J. Fluid Mech.* **645**, 345-373.

[3] Drucker, E.G. and Jensen, J.S. (1996). Pectoral fin locomotion in the striped surfperch. II. Scaling swimming kinematics and performance at a gait transition. *J. Exp. Biol.* **199**, 2243-2252.

[4] Evans, D.H., Piermarini, P.M. and Choe, K.P. (2005). The Multifunctional Fish Gill: Dominant Site of Gas Exchange, Osmoregulation, Acid-Base Regulation, and Excretion of Nitrogenous Waste. *Physiol. Rev.* **85**, 97-177.

[5] Gibb, A.C., Jayne, B.C. and Lauder, G.V. (1994). Kinematics of Pectoral Fin Locomotion in the bluegill sunfish *Lepomis macrochirus*. *J. Exp. Biol.* **189**, 133-169.

[6] Higham, T.E., Day, S.W. and Wainwright, P.C. (2006). Multidimensional analysis of suction feeding performance in fishes: fluid speed, acceleration, strike accuracy and the ingested volume of water. *J. Exp. Biol.* **209**, 2713-2725.

[7] Hughes, G.M. (1960). A comparative study of gill ventilation in marine telosts. *J. Exp. Biol.* **37**, 28-45.

[8] Jones, E.A., Jong, A.S. and Ellerby, D.J. (2008). The effects of acute temperature change on swimming performance in bluegill sunfish *Lepomis marcochirus*. *J. Exp. Biol.* **211**, 1386-1393.

[9] Jones, E.A., Lucey, K.S. and Ellerby, D.J. (2007). Efficiency of labriform swimming in the bluegill sunfish *Lepomis marcochirus*. *J. Exp. Biol.* **210**, 3422-3429.

[10] Korsmeyer, K.E., Steffensen, J.F. and Herskin, J. (2002). Energetics of median and paired fin swimming, body and caudal fin swimming, and gait transition in parrotfish (*Scarus schlegeli*) and triggerfish (*Rhinecanthus aculeatus*). *J. Exp. Biol.* **205**, 1253-1263.

[11] Lauder, G.V. (1984). Pressure and Water Flow Patterns in the Respiratory Tract of the Bass (*Micropterus salmoides*). *J. Exp. Biol.* **113**, 151-164.

[12] Lauder, G.V., Madden, P., Mittal, R., Dong, H. and Bozkurttas, M. (2006). Locomotion with flexible propulsors: I. Experimental analysis of pectoral fin swimming in sunfish. *Bioisnp. Biomim.* **1**, S25-S34.

[13] Liu, G., Ren, Y., Dong, H., Akanyeti, O., Liao, J.C. and Lauder, G.V. (2017). Computational analysis of vortex dynamics and performance enhancement due to body-fin and fin-fin interactions in fish-like locomotion. *J. Fluid Mech.* **829**, 65-88.

[14] Mittal, R., Dong, H., Bozkurttas, M., Lauder, G.V. and Madden, P. (2006). Locomotion with flexible propulsors: II. Computational modeling of pectoral fin swimming in sunfish. *Bioisnp. Biomim.* **1**, S35-S41.

[15] Mussi, M., Summer, A.P. and Domenici, P. (2002). Gait transition speed, pectoral fin-beat frequency and amplitude in *Cymatogaster aggregata*, *Embiotoca lateralis* and *Damalichthys vacca*. *J. Fish Biol.* **61**, 1282-1293.

[16] Ramamurti, R., Sandberg, W.C., Löhner, R., Walker, J.A. and Westneat, M.W. (2002). Fluid dynamics of flapping aquatic flight in the bird wrasse: three-dimensional unsteady computations with fin deformation. *J. Exp. Biol.* **205**, 2997-3008.

[17] Sfakiotakis, M., Lane, D.M. and Davies, B.C. (1999). Review of Fish Swimming Modes for Aquatic Locomotion. *IEEE J. Oceanic Eng.* **24**, 237-252

[18] Shoele. K. and Zhu, Q. (2010). Numerical simulation of a pectoral fin during labriform swimming. *J. Exp. Biol.* **213**, 2038-2047.

[19] Van Wassenbergh, S. (2015). Solution Strategy to Include the Opening of the Opercular Slits in Moving-Mesh CFD Models of Suction Feeding. *Integr. Comp. Biol.* **55**, 62-73.

[20] Webb, P.W. (1984). Body Form, Locomotion and Foraging in Aquatic Vertebrates. *Amer. Zool.* **24**, 107-120.

[21] Wegner, N.C. and Graham, J.B. (2010). George Hughes and the history of fish ventilation: From Du Verney to the present. *Comp. Biochem. Physiol. Part A* **157**, 1-6.